T. & A. M. Report No. 107

FRETTING FATIGUE STRENGTH

OF

TITANIUM ALLOY RC 130B

BY

H. W. Liu, H. T. Corten and G. M. Sinclair

Sponsored by

General Electric Company
Aircraft Gas Turbine Division
Evendale Plant Laboratory
Cincinnati 15, Ohio
Contract Code No. 46 22 60 333

ABSTRACT

An investigation was made to determine the influence of a number of variables on the fretting fatigue strength of RC 130 B Titanium alloy. The variables studied included different gripping materials, hardness of the gripping materials, gripping pressure, surface preparation of specimens, dry lubricants, metallic coatings and special screen gripping shims.

An analysis of experimental results suggests that the primary mechanism responsible for fretting fatigue damage is the repeated frictional shear stress on the asperities or surface "high spots" which are in contact. The frictional force is influenced by cold welding or alloying tendency and by surface roughness.

Based on prevention of fatigue crack initiation by this mechanism, a mathematical expression is proposed which relates the fretting fatigue strength to the fatigue limit of the specimen material, the hardness of the gripping material and the coefficient of friction.

ACKNOWLEDGMENT

This investigation was conducted in the Fatigue of Metals Laboratory of the Department of Theoretical and Applied Mechanics as a part of the work of the Engineering Experiment Station, University of Illinois, in cooperation with the Evendale Plant Laboratory of the General Electric Company under Contract Code No. 46-22-60-333. Special acknowledgment is due to Professor T. J. Dolan, Head of the Department, for his criticism and helpful discussion. Acknowledgment is due to J. Campbell, M. Capehart, D. D. Horn, E. F. Kaelble, D. Simroth, J. Stalter, and W. B. Whitler, who assisted in various phases of the project. The assistance and helpful discussions of E. S. Jones, J. D. Marble, T. K. Redden, and R. E. Weymouth of the Evendale Plant Laboratory are also gratefully acknowledged.

TABLE OF CONTENTS

Title Page

Abstract

Acknowledgment

Table of Contents

Index to Tables and Figures

I. Introduction 1

II. Experimental Investigation and Results 3

A. Materials and Specimens 3

B. Experimental Apparatus and Procedures 4

C. Experimental Results 5

1. Gripping Pad Hardness 7

2. Gripping Pressure 8

3. Oxidation 8

4. Special Surface Preparations 9

III. Discussion of Results 10

A. Model of Mechanical Mechanism of Fretting Fatigue Crack Initiation 10

1. Gripping Pad 13

2. Specimen 13

B. Gripping Pad Hardness 14

C. Gripping Pressure 19

D. Oxidation 20

E. Special Surface Preparations 21

F. X-Ray Study of Debris 23

IV. Conclusions 24

TABLE OF CONTENTS (CONT'D)

Appendix 1	Estimation of Maximum Slip Between the Specimen and the Gripping Pad.	26
Appendix 2	X-Ray Diffraction Test of Fretting Debris	28
References		30
Tables and Figures		

Figures

Fig. 1	Fatigue Specimens and Gripping Pads
Fig. 2	(a) Schematic Diagram
	(b) Photograph of the Experimental Set-up
Fig. 3	Fretting Fatigue Strength of RC 130B Titanium Alloy Under Various Experimental Conditions
Fig. 4	S-N Diagrams for Various Experimental Conditions
Fig. 5	Influence of Hardness of Gripping Pads on Fretting Fatigue Strength
Fig. 6	Influence of Gripping Pressure on Fretting Fatigue Strength
Fig. 7	Contacting Asperities and Associated Stresses
Fig. 8	Dimensionless Diagram Showing Fatigue Strength as Influenced by the Fatigue Limit of the Material, the Hardness of the Gripping Pads, and the Coefficient of Friction
Fig. 9	S-N Curve for RC 130B Titanium Alloy, Mechanically Polished Surface
Figs. 10-32	Fretting Fatigue Data for RC 130B Titanium Alloy

Tables

Table 1	Chemical Compositions of Materials
Table 2	Surface Preparation of Specimens
Table 3	Summary of Results
Table 4	X-Ray Diffraction Patterns of Fretting Debris
Table 5	Compositions of Fretting Debris Determined by X-Ray Diffraction Test

I. INTRODUCTION

Fretting or fretting corrosion are terms commonly employed to describe the surface damage that occurs when two members, pressed in contact, undergo small repeated sliding or relative motion. Shrink or press fits, bolted or riveted joints subjected to repeated loads and ball bearings subjected to small oscillatory motion, are just a few examples of members that often exhibit surface damage and debris dust due to fretting. The fretted surface exhibits characteristics very similar to wear, including abrasion, metal transfer, and often increased roughness and pitting (1, 2)*. In addition, chemical oxidation products (debris and compacted surface layers) generally accompany fretting in air (2).

Fretting damage to a metal surface results in a reduced fatigue strength. In the past, this reduction in strength has been accounted for by employing a liberal factor of safety. Recent emphasis on the strength/weight ratio, introduction of new materials, and more severe operating conditions in the aircraft and automotive industries, all accentuate the importance of the fretting fatigue problem.

General agreement has not been reached with regard to the relative contributions of mechanical and chemical action in causing fretting damage. Chemical (2, 3), mechanical (1, 4), and combined chemical and mechanical mechanisms (5), have been given as the primary cause of fretting. Much of the experimental work on fretting damage has been done on steel. When fretting occurs in steel, a reddish oxide, largely of the composition of Fe_2O_3, is formed (5). This fact has prompted the theory that a chemical mechanism is the cause of fretting damage.

---

* Numbers in parentheses refer to the references in bibliography.

Recent work on non-metallic and non-ferrous materials (1, 6, 7) such as mica, glass, gold, copper, aluminum, etc., several of which are non-oxidizing, demonstrates that fretting damage persists in these experiments; therefore, a mechanical component or mechanism of fretting damage appears necessary.

Fretting damage has been measured in terms of weight loss (5), severity of surface damage by visual observation (1, 2), and reduced fatigue strength (8, 9, 10). In terms of weight loss, the fretting damage increases with an increase of gripping pressure (5), and increase in the relative slip displacement (5), and a decrease in cyclic frequency for a given number of cycles (5). In a vacuum or an inert gas atmosphere, the fretting damage in terms of severity of surface damage is greatly reduced for steel (2); further, humidity has considerable influence on the weight loss (5, 11).

In terms of reduced fatigue strength, the fretting damage increases rapidly as the gripping pressure is increased in the low pressure range. At gripping pressures greater than 5000 psi, the fretting damage remains fairly constant (10). Changes of geometric shape of the specimen may result in a beneficial effect (8, 12) and cold working of the specimen surface is also a partial remedy for alleviating fretting fatigue damage (8, 9, 12), but lubrication has not been effective (8).

This study was undertaken to clarify the mechanism of fretting fatigue damage and to suggest practical remedies to the problem. The material used for all fatigue specimens was RC 130B titanium alloy. The influence of such variables as gripping pressure, gripping pad materials, and specimen surface treatment were studied. Magnesium, several aluminum alloys, copper, brass, titanium alloy, and steel of

several hardnesses were used as gripping pad materials. Surface treatments of the titanium included oxidizing, shot peening, teflon coating, tungsten carbide plating, and aluminizing. To explore the influence of oxidation and debris in causing failure, some fretting fatigue tests were conducted in an atmosphere of dry argon, and in other experiments nickel-coated copper screens were employed as inserts or cushions between the gripping pads and the specimens.

II. EXPERIMENTAL INVESTIGATION AND RESULTS

A. Materials and Specimens

All fretting specimens were made of titanium alloy RC 130B which was received as 1/2" x 3/8" rectangular rod. The mechanical properties were determined to be:

Tensile Strength = 162,000 psi

Yield Strength (tensile) = 149,700 psi

Elongation = 16.5 per cent (2 in. gage length)

The chemical composition of the titanium alloy used is given in Table 1. Nine materials were used as gripping pads. They were commercially pure magnesium and aluminum, aluminum alloys, 1100-F, 2011-T8, and 7075-T6, copper, 70-30 brass, RC 130B titanium alloy, Lapelloy (martensitic stainless steel), and SAE 4340 steel. The chemical composition of the various gripping pad materials is also presented in Table 1.

The mating surfaces of all the steel pads were finished by grinding, and all the non-ferrous pads were mechanically polished. Specimen surfaces as mechanically polished, oxidized, shot peened, teflon coated, tungsten-carbide flame plated, and aluminized were tested. The preparation of these surfaces is described briefly in

Table 2. Also nickel plated copper screens of 40 and 80 mesh sizes were used as inserts or cushions between the specimen and the SAE 4340 steel pads.

Two types of fretting fatigue specimens were used as illustrated in Fig. 1a and 1b. The specimens shown in Fig. 1a were used throughout most of this investigation. In a few of the experiments, stresses nearly equal to the fatigue limit of the material were employed; therefore, the specimen shown in Fig. 1b was used to avoid an occasional failure away from the test section. The specimen shown in Fig. 1b has a gradual increase in cross-section in both dimensions a short distance away from the contact area. The gripping pads are shown in Fig. 1c, and the conventional fatigue specimen used to determine the fatigue limit for the material with a mechanically polished surface is shown in Fig. 1d.

B. Experimental Apparatus and Procedures

In Figs. 2a and 2b, a schematic diagram and a photograph of the fretting fixture and experimental set-up are shown. Specimen A was gripped between two pads, B, by a normal force applied through the steel beam, C, by screws K. This normal force was determined from the deflection of the calibrated beam, C, using dial, D.

The specimen was rigidly connected to the horizontal loading arm F. The bending moment was applied by an eccentric cam H through the vertical loading crank G. Dial I was used to adjust and set the cam by reproducing the deflection corresponding to the desired stress as determined from a static load calibration.

Due to the repeated bending stress, slip occured between the specimen and the gripping pads. In Fig. 2a, L is the location of

the maximum repeated slip. The slip was estimated to be of the order 10^{-4} to 10^{-5} inches, and the method of estimation is presented in Appendix 1.

In all of the experiments, the mating surfaces were carefully cleaned with acetone prior to the assembly of the fixture. In one series an argon atmosphere was employed. A rubber container was used to cover the specimen and part of the machine. Argon was forced through heated steel wool to extract traces of oxygen before the gas was fed into the test chamber. The gas was fed through the container for a half hour period before the repeated load experiment was started to remove traces of air. A back pressure of 1/2" water was maintained throughout the test to insure that air did not leak into the test chamber.

A life of 5×10^7 cycles was defined as a run-out for all fretting fatigue experiments, and a life of 2×10^7 cycles was defined as a run-out for conventional fatigue experiments. Nine Krouse plate fatigue machines operating at 1800 rpm were used in this investigation.

The fretting debris from several series of experiments was examined by X-ray to determine its composition. The debris was taken either from the specimen or the gripping pads. It was examined by an ordinary X-ray powder diffraction camera. A more detailed description of the method and results is given in Appendix 2.

C. Experimental Results

Table 3 summarizes the fatigue results for all of the experimental conditions. A series number was assigned to each experimental condition and is listed in the first column of Table 3. For convenience, it will be used to designate that condition throughout this report instead of repeatedly describing the detailed test conditions. The second column lists all of the gripping pad materials. The third and fourth columns

give the Vicker's hardness numbers for gripping pads and specimens, respectively. Loads ranging from 2 kg. for the very soft metals to 10 kg. for the hard metals were used to measure the hardness. Each hardness value in Table 3 represents the average of ten readings. The nominal gripping pressure, which does not take stress concentration and slight changes of gripping pressure due to repeated bending into consideration, is listed in column 5. Column 6 lists the surface preparations; a more detailed description is included in Table 2. The fretting fatigue strengths for each experimental condition are listed in column 7. Since the term "fretting fatigue strength" will be used repeatedly, it will be called simply 'strength' hereafter.

Fig. 3 shows the 'strength' arranged with decreasing 'strength' toward the right, for all of the different experimental conditions. It is evident that the 'strengths' for essentially identical specimens vary over a considerable range depending upon the gripping pads and surface treatment of the specimens. The highest 'strengths' were approximately equal to the fatigue limit of the material and occured with the very soft gripping pad materials. The lowest 'strengths' were approximately 0.20 of the fatigue limit of the material and occured when hard gripping pads were employed. Many of the special surface treatments resulted in 'strengths' intermediate between the extreme values. The S-N diagrams for each experimental condition are presented in Figs. 9-32.

In Fig. 10 and 11, Series 2 and 3, with magnesium and aluminum 1100-F pads, 'strengths' higher than the fatigue strength of the material are indicated. Actually in the process of repeated loading, the soft gripping pads yielded and were slightly worn away. Therefore,

the real stress developed in the specimen after the first few thousand cycles, was somewhat lower than the original stress. To measure this, recalibrations were made on two specimens using magnesium and aluminum 1100F pads which were originally set up at a stress of 90,000 psi. After run-out, the re-calibration gave stresses of 74,000 psi and 86,000 psi, respectively.

In Fig. 4, the combined S-N curves are shown for only the mechanically polished surface specimens under various experimental conditions. It appears that these curves can be divided into two groups. The top group shows little effect of fretting. The bottom group exhibits 'strengths' that are reduced to a range from 0.2 to 0.4 of the fatigue limit of the material.

Also in Fig. 4, the 'knee' of most of the S-N curves occurred near a life of 3×10^6 cycles. However, for copper and brass pads, series 6 and 7 respectively, the specimens had unusually long lives, and these two curves were shifted to the extreme right. Whether the 'knee' in these curves actually exists is not known. The long time that would be required to establish a 'knee' in the range of 5×10^7 cycles was prohibitive.

In the following paragraphs, the variables that influence the 'strength' have been isolated to aid in evaluating these factors.

1. Gripping Pad Hardness

Fig. 5 shows the influence of the hardness of the gripping pads on the 'strength' of mechanically polished specimens.* The 'strength' decreased rapidly from 89,000 psi to the range of 20,000 to 30,000 psi as the gripping pad hardness was increased from 0 to 200 VHN, but remained essentially constant as the gripping pad

---

* In this figure, the 'strengths' of Series 2 and 3 were arbitrarily adjusted to 85,000 psi.

hardness was increased beyond 200 VHN. The three smooth curves in this figure, are based on the analytical work and will be discussed in Section III B.

2. Gripping Pressure

In test series 10, 11, 12 and 14, gripping pads of SAE 4340 steel with a hardness 397 VHN were employed. Nominal gripping pressures were used which ranged from a minimum of 4000 psi to a maximum of 60,000 psi. As indicated in Fig. 6, the 'strength' decreased very rapidly as the gripping pressure was increased from zero (no fretting), until at a gripping pressure at 4000 psi, the 'strength' was only 28,000 psi or approximately 31 per cent of the fatigue limit of the material. As the gripping pressure was increased above 4000 psi, the 'strength' decreased only slightly. At 60,000 psi gripping pressure, the strength was 18,000 psi, or 20 per cent of the fatigue limit of the material. Thus, a 15 fold increase in gripping pressure produced only an additional 11 per cent decrease in the 'strength'.

3. Oxidation

The experimental conditions of series 16 included an argon atmosphere, but in all other aspects it was identical to series 13 which was run in air. The 'strengths' for these two series were the same, but the fatigue life in the argon atmosphere was slightly longer than in the air.

Series 17 used specially oxidized specimens (see Table 2). The estimated thickness of the oxide layer was of the order of 1×10^{-4} inch. Two batches of specimens were prepared. Specimens of batch 1 were immersed in hydrogen peroxide for two hours, while the specimens

of batch 2 were immersed for 16 hours. The 'strength' of batch 1 was 50,000 psi, and the 'strength' of batch 2 was somewhat lower, but was not completely determined due to a shortage of these specimens. In Fig. 25, two sets of data symbols were used to denote the two different batches. The other experimental conditions of this series were similar to those of series 11 and 13, but the 'strength', 50,000 psi for batch 1 was 140% higher.

4. Special Surface Preparations

Two series of shot peened specimens were investigated. The specimens of series 18 were shot peened using P39 steel shot at 75 psi air pressure. Aluminum alloy 7075-T6 gripping pads were used and a 'strength' of 55,000 psi was obtained at the defined run-out life. However, as shown in Fig. 26, the 'knee' of S-N curve did not occur within this life.

The specimens of series 19 were shot peened by P19 steel shot. SAE 4340 steel pads of 238 VHN were used. The 'strength' was 48,000 psi and the 'knee' occurred at a life of 10^7 cycles.

Series 20 employed teflon-coated specimens. The 'strength' was improved to 51,000 psi.

In series 21, tungsten carbide flame plated specimens and pads resulted in a 'strength' of 21,000 psi. In the process of flame plating, the tungsten carbide particles were detonated to a supersonic velocity and were embedded in the surface of the specimen. The coating appeared to adhere well to the surfaces and was 0.002 in. thick after grinding. The fatigue fracture was perpendicular to the surface and no tendency for separation of the plating was noticed.

In series 22, an aluminized surface was used. The estimated thickness of the aluminum layer was approximately 0.003 inches. In the coating process, the specimens were aluminized at a temperature of 1350°F for 4 minutes, and subsequently were subject to a diffusion temperature of 1900°F for 15 minutes. The 'strength' was 22,000 psi.

Nickel plated copper screens were inserted between the steel gripping pads (238 VHN) and the mechanically polished specimens in series 23 and 24. Screen mesh sizes of 40 and 80 were used for series 23 and 24, respectively. The 'strengths' were improved to 44,000 psi with the 40 mesh screen, and 34,000 psi with the 80 mesh screen.

III. DISCUSSION OF RESULTS

A. Model of Mechanical Mechanism of Fretting Fatigue Crack Initiation

The modern theory of friction and wear is based on the fact that when two metal surfaces are pressed into contact, only the high asperities of these two surfaces actually contact (13). These asperities yield and cold weld together as shown schematically in Fig. 7a and 7b. When the two surfaces undergo a relative lateral displacement, these welded asperities break either at the inter-face or within the asperities. The failure may similate that of static fracture if the relative velocity is low and the displacement is large; or if the displacement is repeated and small, thousands of cycles of loading may be necessary to produce progressive fracture (fatigue) of the asperities.

If the strengths of the two mating metals are different, the weaker surface will be damaged severely, and the stronger surface may or may not be damaged depending on the statistical distribution of the strengths of the asperities. If the strongest asperity of the weaker surface is weaker than the weakest asperity of the stronger surface, there will be no damage to the stronger metal surface. Otherwise the stronger surface may be damaged also.

With the present experimental set-up, welded asperities near the edge L, as shown in Fig. 2a, due to the relatively large displacement, will break with one or several cycles of loading. If the failure takes place through the specimen asperities, the surface will be roughened and the fatigue strength will be reduced, but not to the extent of 0.2 of the fatigue limit of the material as reported in the previous section.

At locations away from the edge of the grip, the relative lateral displacement, which induces the repeated frictional shear stress between these two surfaces, decreases. It is in this region that fatigue damage and progressive fracture have been observed to occur (8). The present experiments confirm previous findings (8) that the location of failure is not at the edge of the grip, but rather it is at a short distance inside of the grip. This repeated frictional shear stress together with the repeated bending stress at a particular location initiates fatigue cracks and cause fatigue damage. The welded asperities apparently develop small cracks only after thousands cycles of loading have been applied.

By considering the fully plastic condition of the weaker asperities, governed by the coefficient of friction and the yield pressure of the weaker of the two mating metals, the maximum repeated frictional shear stress that can be developed at the interface may be estimated. If the combined influence of the frictional shear stress and the bending stress is larger than the fatigue limit of the specimen material, fatigue cracks will be initiated. In the analysis of the stresses on the specimen and the gripping pad asperities that follows, it will be shown that the 'strength' is related to the fatigue limit of the specimen material, the hardness of the gripping pad, and the coefficient of friction. The Vicker's hardness number bears a definite relation with the yield pressure of the material (14). While it is not a necessary requirement, it will be assumed for convenience of presentation that the yield strength of the gripping pad material is lower than that of the specimen material. The following symbols will be used in the analysis:

τ_{max} — maximum shear stress in the asperities of gripping pad, psi

p — normal pressure on the asperities, psi

μ — coefficient of friction

P — yield pressure of the weaker metal in the fully plastic state, psi

σ_y — yield strength of the weaker material, psi

H — Vicker's hardness number of gripping pads, Kg/mm^2

τ_{alt} — alternating shear stress in specimen due to alternating bending stress and frictional shear stress, psi

σ_{alt} — alternating bending stress in specimen, psi

1. Gripping Pad

Fig. 7c shows the stresses acting on an infinitesimal block of the material of the gripping pads at the inter-face. The maximum shear stress on the block is:

$$\tau_{max} = p\sqrt{\left(\frac{1 - k}{2}\right)^2 + \mu^2} \qquad (1)$$

From the two-dimensional solution of an ideal plastic metal loaded by a flat punch without friction, k is equal to $\frac{\pi}{2 + \pi}$ * (14). For the fully plastic condition of the asperities, τ_{max} is equal to the shearing yield strength of the gripping pad material, i.e. $\tau_{max} = \sigma_y/2$. Using the following relationships (14),

$$P = 3\sigma_y$$

$$P = 1420 \times \frac{H}{0.927}$$

and Eq. 1, the following expression between p, H and μ is obtained:

$$p^2 = 2.61 \times 10^5 \frac{H^2}{0.151 + 4\mu^2} \qquad (2)$$

where 1420 is the conversion factor for Kg/mm^2 to psi, and p is the maximum normal pressure that the pad asperities can sustain in a fully plastic state, when a frictional shear stress μp and normal pressures p and kp are superimposed.

2. Specimen

Fig. 7d shows the stresses acting on an infinitesimal block of material of the specimen at the inter-face. On plane AC, when σ_{alt} is tensile, the shear stress, τ_1, is equal to

---

* To use the value of k for the solution of a flat punch without friction introduces error, but this analysis shows that the error is negligible, if μ is equal to or larger than 0.5.

$$\tau_1 = \frac{1}{2}(1 - k)\, p \sin 2\theta - \mu p \cos 2\theta + \frac{1}{2}\sigma_{alt} \sin 2\theta$$

When σ_{alt} is compressive, the shear stress, τ_2, is equal to

$$\tau_2 = \frac{1}{2}(1 - k)\, p \sin 2\theta + \mu p \cos 2\theta - \frac{1}{2}\sigma_{alt} \sin 2\theta$$

The amplitude of the repeated shear stress, τ_{alt}, is equal to

$$\tau_{alt} = \frac{1}{2}(\tau_1 - \tau_2)$$

$$= \sigma_{alt} \sin 2\theta - 2\mu p \cos 2\theta$$

The maxima of τ_{alt} with respect to θ was determined to be

$$\tau_{alt} = \frac{1}{2}\sqrt{4\mu^2 p^2 + \sigma_{alt}^2} \qquad (3)$$

By setting τ_{alt} equal to the shearing fatigue limit (1/2 of bending fatigue limit) of the specimen material and using Eq. 2 for the value of p, Eq. 3 can be solved for σ_{alt}, the allowable bending stress, in terms of τ_{alt}, H, and μ, to be:

$$\sigma_{alt} = \sqrt{4\tau_{alt}^2 - 1.04 \times 10^6 \frac{\mu^2 H^2}{0.151 + 4\mu^2}} \qquad (4)$$

Eq. 4 gives the limiting values of σ_{alt} for preventing fatigue crack initiation, and indicates that, for a given gripping pad hardness, the 'strength' σ_{alt}, increases with a decrease in the coefficient of friction. As the coefficient of friction approaches zero, the 'strength' approaches the fatigue limit of the specimen material.

B. Gripping Pad Hardness

For particular values of μ and H, fatigue cracks will be initiated if the applied repeated bending stress is higher than σ_{alt}

given by Eq. 4. If σ_{alt} is lower than the value given by Eq. 4 no fatigue cracks will be initiated, and fatigue failure will not occur. Based on Eq. 4, three curves were drawn in Fig. 5 corresponding to values of μ of ∞, 0.3, and 0.2, and using $\tau_{alt} = 1/2\ (89,000) = 44,500$ psi. For a range of values of μ from 1 to ∞ the curves are nearly identical and result in a shift in the horizontal intercept (hardness) of the curves of only 2 per cent. As the value of μ decreases from 0.2 to 0, the horizontal intercept moves rapidly to the right. However, the equations become less reliable for low coefficient of friction due to the error introduced by the value of k in Eq. 1. The curve for μ equal to ∞ was plotted and this curve can be used for all values of μ that are greater than 1. For most practical applications, the range of coefficients of friction is from 0.2 to 3. Thus, the band bounded by curves for μ equal 0.2 and ∞ indicates the general relationship between the gripping pad hardness and the 'strength'. The most rapid drop in the 'strength' occurs within the critical hardness range of 100 to 230 VHN.

Fig. 5 shows that, for any given value of σ_{alt} and μ, there is an upper limiting value of hardness, H, to avoid fatigue crack initiation. If H is higher than this limit, fatigue cracks will be initiated. Once a crack is initiated, it may propagate into the specimen. As the depth of the crack increases, the amplitude of the repeated frictional shear stress, μp, decreases rapidly and approaches μN, or a value even lower than μN, where N is the gripping pressure*. Therefore, the

---

* If the frictional shear stress at all the contacted asperities, longitudinally across the contact area was μp, the shear stress beneath the surface would approach μN. If the frictional shear stress at the asperities near the edge L, Fig. 2a is μp, but decreases to zero toward the left edge; the shear stress beneath the surface will approach a value lower than μN.

repeated bending stress, σ_{alt}, becomes the main component of the repeated stress which propagates the crack. The fretting fatigue member will not fail, if the resultant of the repeated bending stress and the surface friction induced shear stress, at a certain depth beneath the surface, is lower than the stress necessary to propagate the crack. In other words, if the hardness of the gripping pad is higher than the limiting value prescribed in Fig. 5, fatigue cracks will be initiated at the surface, and the 'strength' will be determined by the bending stress at which the fatigue cracks cease to propagate.

As the hardness of gripping pads increases, the actual contact area between pad and specimen decreases, and the frictional shear stress, μp, becomes larger. Consequently, at a given depth beneath the surface, the shear stress will be higher, since the surface frictional shear stress, μp, is higher. Obviously this effect is rather small. However, the alternating bending stress that is necessary to propagate a crack decreases slightly with an increase of the hardness of the gripping pads, i.e. the 'strength' decreases slightly with an increase in gripping pad hardness. Based on the experimental data, a straight line was drawn through the data in Fig. 5. For $\mu = 0.3$, this straight line intersects the curve governing crack initiation, Eq. 4, at point A. If the gripping pad hardness is lower than the abscissa of A, the 'strength' is governed by crack initiation. If the gripping pad hardness is higher than the abscissa of A, the 'strength' is governed by crack propagation.

Considering the normal scatter of fatigue data, the variation of gripping pressure employed in the different test series, and the

simplifications and assumptions made in the analysis, the experimental data shown in Fig. 5 fit the general pattern of the analytical curves very well. The data for series 4, 7, and 8 show the greatest deviations. Whether these deviations are due to unusual scatter of the data or due to the simplifications made in the analysis is not known. It does appear, however, that the relationship between 'strength', that is either crack initiation or propagation, and hardness is adequately verified by the data.

The simplifications and assumptions made in the analysis may be enumerated as follows:

(a) The ratio between the yield pressure and the yield strength was assumed to be 3. Actually, this ratio can vary from 2.6 to 3.3 depending upon the state of cold work of the asperities (14).

(b) A super-imposed static compressive stress does not affect the fatigue strength of the material. The available evidence generally supports this assumption (15), however, the state and magnitude of the super-imposed static compressive stress encountered in the fretting specimens was somewhat different from any that have been investigated.

(c) Any influence of the debris particles was neglected. These particles may possibly act as a solid lubricant or as an abrasive. The alloying effect (16, 17) between the two mating surfaces was neglected. Alloying definitely changes the surface properties, such as coefficient of friction, hardness, strength, etc. The change of the surface hardness of the specimen and the gripping pads due to cold working during repeated sliding was neglected. A change in surface hardness could result in a change in the surface fatigue strength.

One or a combination of these factors may account for the deviations noted in series 4, 7, and 8. It is interesting to note that in test series 6 and 7, in which the data in Fig. 5 lie to the left and below the solid curves, copper or copper base alloy gripping pads were used. By comparison, series 4 and 5 which employed aluminum alloy pads, showed higher 'strength' for higher hardness. This observation correlates with a previous finding using similar pad materials and steel specimens (18).

Eq. 4 may be rearranged in the dimensionless form,

$$\left[\frac{1420\,H}{2\tau_{alt}}\right]^2 = 1.933\left[1-\left(\frac{\sigma_{alt}}{2\tau_{alt}}\right)^2\right]\left[\frac{0.151}{\mu^2+4}\right] \quad (5)$$

If the dimensionless quantities, $\frac{\sigma_{alt}}{2\tau_{alt}}$ and $\frac{1420\,H}{2\tau_{alt}}$, are plotted as ordinate and abscissa respectively for various values of μ, as shown in Fig. 8, the curves based on Eq. 5 can be used for other materials, independent of the value of τ_{alt}. Results for steel specimens with low hardness gripping pads (18) were found to fit the dimensionless plot, as shown in Fig. 8 by the solid square points. However, the value of the ratio $\frac{\sigma_{alt}}{2\tau_{alt}}$, for which cracks cease to propagate, that is the 'strength' for $\frac{1420\,H}{2\tau_{alt}} > 4.0$, appears to depend upon the specimen material. More work in this area is desirable.

If a linear relationship is assumed between H and σ_{alt} for fatigue crack propagation, the extrapolation of the straight line of Fig. 5 to H = 0 gives the stress that is necessary to propagate a crack in the absence of fretting. The value was approximately 30,000 psi.

Based on the above analysis, the general remedies for fretting

fatigue damage and reduced fatigue strength can be summarized to be: (a) reduce the gripping pad hardness below the critical hardness range (b) reduce the coefficient of friction to a value below 0.1 (c) increase the stress that is necessary to propagate a fatigue crack, and (d) prevent metal to metal contact.

C. Gripping Pressure

It is obvious, from the above analysis, that the frictional shear stress, μp, is independent of gripping pressure, because p depends only on the hardness of gripping pad, H, and the coefficient of friction, μ. Since the initiation of fatigue cracks depends on μp and σ_{alt} only, it is also independent of gripping pressure. However, the surface friction induced shear stress beneath the surface of the specimen is related to μN. It increases with the gripping pressure. Since the propagation of a crack depends on the resultant of the surface friction induced shear stress and the bending stress σ_{alt}, an increase in the surface friction induced shear stress decreases the bending stress σ_{alt} that is necessary to propagate a crack. The surface friction induced shear stress component is small. Consequently, an increase in gripping pressure decreases the 'strength' only slightly. Fig. 6 shows the experimental results. The decrease in 'strength' is very small with respect to the increase in gripping pressure. A 15 fold increase in gripping pressure, resulted in only an additional 11 per cent decrease in 'strength'. If a linear relationship between gripping pressure and 'strength' is assumed, extrapolation to zero pressure gives the stress that was necessary to propagate the fatigue cracks in the absence of fretting. Extrapolation gave a value of approximately 30,000 psi which is about the same as the value obtained

by extrapolation of the straight line in Fig. 5 to zero hardness.

D. Oxidation

A comparison of the results of test series 16, 13, and 17, indicates the influence of an oxide layer on the surface of the specimen. Series 16, which employed an argon gas atmosphere, gave a 'strength' of 21,000 psi, the same as that of series 13 which was run in air. This result agrees with the interpretation of the proposed hypothesis of fatigue damage at the cold welded asperities by the repeated bending stress and the super-imposed repeated frictional shear stress.

In series 17, deliberately oxidized specimens were used. The 'strength' of batch 1 specimens, 50,000 psi, was approximately 240 per cent of that of series 13, in which comparable experimental conditions were used except for the thickness of the oxide layer. Batch 2, which was oxidized for a longer time, exhibited a lower (but undetermined) 'strength' than batch 1. The increased strength of batch 1 is presumably due to the thicker protective oxide layer. The thick oxide layer prevents clean metal contact and solid phase welding, and reduces the coefficient of friction, possibly in a manner similar to a solid lubricant. The lower coefficient of friction reduces the repeated frictional shear stress which is the main component of the repeated stress on the specimen asperities. Consequently, the protective functioning of the oxide layer apparently depends on the properties of the oxide, that is, the volumetric change of the layer during the oxidizing process, the bond between the oxidized layer and the base metal, preferential attack of the surface, and the thickness of the layer.

The results of test series 16 and 17 suggest that the occurance of oxidation during the progress of the experiment is an insignificant part of the surface damage when fretting is measured in terms of fatigue strength.

E. Special Surface Preparations

These surface preparations include shot peening, teflon coating, tungsten carbide plating, aluminizing, and the use of nickel plated copper screens as inserts or cushions between the gripping pads and the specimen.

Shot Peening

The specimens of series 18 and 19 were shot peened, each series with a different size shot. The gripping pad materials were Al 7075-T6 and Steel SAE 4340, respectively. The 'strength' was improved to 55,000 and 48,000 psi respectively. The 'knee' of S-N curve did not appear in series 18, within the run-out life of 5×10^7 cycles.

The shot peening process cold worked the specimen surface and apparently raised the stress necessary to initiate as well as to propagate cracks. It is presumed that cracks were initiated by the proposed mechanism and the 'strength' of series 19 was the stress at which the cracks ceased to propagate.

The long life of these specimens, particularly series 18, may be attributable to the slow propagation of the cracks within the cold worked layer.

Teflon Coating

Series 20, the teflon coated specimens, gave a 'strength' of 51,000 psi. Teflon has a low coefficient of friction and exhibits

a strong bond with the base material. Initially, at least, it serves as a buffer between the two metal surfaces and prevents metal to metal contact. However, teflon will be gradually worn away (19). If the coating is worn off, metal to metal contact will take place again, and in this case the increased repeated frictional shear stress may reduce the 'strength'. Therefore, the protection afforded by a teflon coating appears to be dependent upon the thickness of the coating and the desired life of the part.

Both shot peening and teflon coating appear to offer practical remedies that reduce the fretting damage.

Tungsten Carbide Flame Plating

Series 21, the tungsten carbide flame plated specimens, gave a strength of 21,000 psi. Whether this reduced strength was due to the metallurgical change of the material or surface damage during the processing needs more exploratory study. Another possible explanation is that the strength of the coating is low, and cracks within the coating serve as notches in the specimen (20).

Aluminizing

In view of the high 'strengths' of series 3 and 4, it was thought that if a layer of aluminum were applied to the specimen and the Lapelloy pads, the Lapelloy-titanium contact would be prevented, and the strength will be increased. Therefore, test series 22 was conducted using aluminized specimens. A 'strength' of 22,000 psi was obtained.

This reduced 'strength' is believed to be due to the fact that the coating was too thin and was worn away. The thickness of the aluminized and the oxide layers were very similar, but they served

different functions. The oxide layer reduced the coefficient of friction and thereby reduces the repeated frictional shearing stress.

The aluminum layer served as a buffer between the gripping pads and the specimen. However, the soft layer was apparently too thin and was rapidly worn off; consequently, no beneficial increase of 'strength' was obtained. The alloying effect between the aluminum and the titanium and the high temperature during the aluminizing process also may have affected the 'strength'.

Screens

The nickel plated copper screens resulted in an increased 'strength'. The reason for this improvement is not well understood since the screen may function in several ways. The increased 'strength' may be due to the low hardness of the nickel and copper, or due to the fact that the relative lateral displacement between the gripping pad and the specimen was partially absorbed by the screen. In the latter case, the relative displacement between the screen and the specimen asperities may have been reduced to the point that an increased bending stress was necessary to cause fatigue failure.

If debris particles are at all significant, the open grid of the screen certainly offers ample space to remove the particles from critical regions.

F. X-Ray Study of Debris

The fretting debris from test series 2, 3, 6, 7, and 9 were analyzed by X-ray to determine its composition. The results are summarized in Table 5. For test series 2, 3, and 6, which gave strengths ranging from 85,000 psi to 72,000 psi, the results showed that no titanium or titanium alloy was detected. The results

of series 7 and 9, which gave strengths of 30,000 psi and 24,000 psi respectively, show that the debris includes titanium alloy. This indicates that if a high 'strength' was obtained, the gripping pads did not damage the specimen. Conversely, if a low 'strength' was obtained, the X-ray analysis indicated that the specimen surface was damaged, that is, titanium in some form was found in the debris. These results are in agreement with the proposed mechanism of fatigue crack initiation discussed previously.

IV. CONCLUSIONS

The results of this investigation appear to justify the following conclusions:

1. Severe fretting damage reduces the fatigue strength of RC 130B titanium alloy to as low as 0.2 of the fatigue limit of the alloy.

2. The mechanism responsible for fretting fatigue damage appears to be the repeated frictional shear stress on the contacted asperities of the specimen surface. Based on prevention of fatigue crack initiation by this mechanism, a mathematical expression was derived which relates the fretting fatigue strength to the fatigue limit of the specimen material, the hardness of the gripping pad, and the coefficient of friction. The experimental data are in good agreement with the analytical expression.

3. To reduce the severity of fretting damage and increase the fretting fatigue strength, the analysis suggests the following remedies: (a) reduce the gripping pad hardness below the critical hardness range of 100 to 230 VHN, (b) reduce the coefficient of friction below 0.1, (c) increase the stress that is necessary to

propagate a fatigue crack, and (d) prevent metal to metal contact.

4. Fretting caused by gripping pads of hardness above the critical range, reduce the fretting fatigue strength to the range of 0.2 to 0.4 of the fatigue limit of the titanium alloy specimens. Gripping pads of low hardness, below the critical range, give fretting fatigue strengths above 0.8 of the fatigue limit of the specimen.

5. Special surface treatments employing either an oxidized layer or teflon coating increase the fretting fatigue strength to approximately 0.56 of the fatigue limit of the alloy. The oxidized layer and the teflon coating each prevent metal to metal contact and are believed to reduce the coefficient of friction.

6. Shot peening improves the fretting fatigue strength to 0.5 to 0.6 of the fatigue limit of the titanium alloy. Shot peening is believed to increase the stress that is necessary to propagate a crack.

7. Exclusion of an oxygen (or air) atmosphere did not result in an improved fretting fatigue strength.

8. The two surface treatments, tungsten carbide plating and aluminizing, resulted in no increase of the fretting fatigue strength.

9. Using nickel plated copper screen as inserts or cushions between the gripping pad and the specimen, increased the fretting fatigue strength slightly.

Appendix 1 - Estimation of Maximum Slip Between the Specimen and the Gripping Pad.

When the specimen was bent repeatedly, the upper and the lower fibers of the specimen elongated and contracted alternatively. A minute slip between the specimen and the gripping pads occurs near the edge, L, Fig. 2a. The maximum slip is at the edge, and it decreases as the location moves into the grip. The slip, e, between the specimen and the gripping pads at the edge is equal to

$$e = \int_0^a \epsilon_x dx$$

where ϵ_x is the unit strain of the element on the surface of the specimen in the x direction at the distance x from L, and a is the distance from the edge, where there is no slip. Assuming the gripping pad is rigid,

$$\epsilon_x = f(\sigma_{alt}, p, \mu, E)$$

where

σ_{alt} = alternate bending stress

p = normal pressure

μ = coefficient of friction

E = Young's modulus of the specimen

The ϵ_x at the edge is equal to σ_{alt}/E. If a is estimated to be 3/8" from a study the debris formation on the gripping pads, and it is assumed that ϵ_x varies linearly with respect to x, and is zero at a, then

$$e = 1/2 \int_0^{3/8} \frac{\sigma_{alt}}{E} dx = \frac{3}{16} \frac{\sigma_{alt}}{E}$$

E is equal to 16×10^6 (21), therefore

$$e = 1.17 \times 10^{-8} \sigma_{alt}$$

If σ_{alt} is 80,000 psi, e is equal to 9.4×10^{-4} in. If σ_{alt} is 30,000 psi, e is equal to 3.5×10^{-4}. The above estimate of slip gives only approximate values, however, it should be correct as to the order of magnitude.

Appendix 2 - X-Ray Diffraction Test of Fretting Debris

X-ray diffraction analysis was employed to study the fretting debris of test series 2, 3, 6, 7, and 9, i.e. with magnesium, Al 1100-F, copper, 70-30 brass, and Lapelloy steel gripping pads respectively. The diffraction patterns were recorded on photographic film by means of a 7 cm. cylindrical camera. The lattice spacings, d, were obtained from Bragg's equation:

$$n\lambda = 2d \sin \theta$$

where

n = order of reflection

λ = wavelength of X-ray

θ = diffraction angle

Two patterns were obtained for each test series: one of filings taken from the gripping material and one of the debris formed at the inter-face. Due to an insufficient amount of debris, a special experimental arrangement was used. All back reflection lines were cut out, but enough transmission lines were obtained in each case to permit comparison of the pattern with either the corresponding filings pattern or the pattern available in the literature. The results are summarized in Table 4 and 5. The debris of series 2, with magnesium pad, was pure magnesium and magnesium oxide. The debris of series 3, with Al 1100-F pad, was pure aluminum. The debris of series 6, with copper pads, consisted of copper and copper oxides. The X-ray diffraction pattern of series 7, with 70-30 brass pad showed one line at 1.64 A^{o} which was not found on the filing pattern. Zinc titanium oxide, $2\,ZnO \cdot Ti\,O_2$, shows a line at 1.63 A^{o}, but it cannot be stated

with certainty that the unexplained line on the deposit pattern was caused by this compound. The debris of series 7 consisted primarily of 70-30 brass and possibly zinc titanium oxide.

As might be expected, no distinct lines appeared on the pattern of the martensitic lapelloy filings. One diffuse line appeared on the deposit pattern, corresponding to a d-spacing of approximately 2.05 A^{o}. The ASTM index lists an iron-titanium compound, $TiFe_2$, having a d-spacing of 2.04 A^{o}. However, the presence of $TiFe_2$ must be regarded as somewhat uncertain.

References

1. Godfrey, Douglas, "Investigation of Fretting Corrosion by Microscopic Observation," NACA Technical Note No. 2039, Feb., 1950.

2. Sakmann, B. W., Rightmire, B. G., "An Investigation of Fretting Corrosion Under Several Conditions of Oxidation," NACA Technical Note No. 1492, June 1948.

3. Fink, M., "Wear Oxidation, A New Component of Wear," Transaction, Am. Soc. Steel Treating, Vol. 18, 1936.

4. Feng, I-Ming, and Rightmire, B. G., "The Mechanism of Fretting," Lubrication Engineering, June 1953.

5. Uhlig, H. H., Feng, I-Ming, Tierney, W. D., and McClellan, A., "A Fundamental Investigation of Fretting Corrosion," NACA Technical Note No. 3029, Dec., 1953.

6. Godfrey, Douglas and Bailey, J. M., "Coefficient of Friction and Damage to Contact Area During the Early Stage of Fretting," NACA Technican Note No. 3011, Sept., 1953.

7. McDowell, J. R., "Fretting Corrosion Tendencies of Several Combinations of Materials," Symposium on Fretting Corrosion, ASTM Special Technical Publication No. 144, 1953.

8. Horger, O. J., "Influence of Fretting Corrosion on the Fatigue Strength of Fitted Members," Symposium on Fretting Corrosion, ASTM Special Technical Publication No. 144, 1953.

9. Horger, O. J. and Maulbetsch, J. L., "Increasing the Fatigue Strength of Press-Fitted Axle Assemblies by Surface Rolling," Journal of Applied Mechanics, Vol. 3, No. 3, Sept., 1936.

10. Thum, A. and Wunderlich, F., "Dauerbiegefestigkeit von Konstrucktionsteilen an Einspannungen, Nabensitzen und ahnlichen Kraftangriftstellen," Mitteilungen der Materialprufungsanstalt an der Technischen Hochschule Darmstadt, Heft 5, VDI - Verlag GMBH, Berlin, 1934.

11. Godfrey, Douglas, "Study of Fretting Wear in Mineral Oil," Lubrication Engineering, Jan. - Feb. 1956, Vol. 12, No. 1.

12. Peterson, R. E. and Wahl, A. M., "Fatigue of Shafts at Fitted Members, With a Related Photoelastic Analysis," Journal of Applied Mechanics, March 1935.

13. Bowden, F. P. and Tabor, D., "The Friction and Lubrication of Solids," Oxford University Press, New York, 1950.

14. Tabor, D., "The Hardness of Metals," Oxford University Press, London, 1951.

15. Smith, J. O., "The Effect of Range of Stress on the Fatigue Strength of Metals," Engineering Experiment Station Bulletin Series No. 334, University of Illinois, Urbana, Illinois, 1942.

16. Machlin, E. S., "Research Points Way to New Methods of Preventing Galling and Seizing," Iron Age, Feb. 10, 1955.

17. Coffin, Jr., L. F., "Study of the Sliding of Metals, with Particular Reference to Atmosphere," Lubrication Engineering, Jan. -Feb., 1956.

18. Corten, H. T., "Factors Influencing Fretting Fatigue Strength," Department of Theoretical and Applied Mechanics, University of Illinois, Urbana, Illinois, 1955.

19. Mason, W. P., and White, S. D., "New Techniques for Measuring Forces and Wear in Telephone Switching Apparatus," Bell System Technical Journal, Vol. 31, p. 469, 1952.

20. Form, G. W., Baldwin, W. M., "The Effect of Brittle Skins on the Ductility of Metals," ASTM Preprint No. 79, 1956.

21. Kaufman, J. G., Crum, R. G., and D'Appolonia, E., "Correlations of the Mechanical Properties of Ti-150A, RC-130A, RC-130B, Ti-Alloy and Ti-75A Titanium Alloys," Interim Report, Civil Engineering Department, Carnegie Institute of Technology.

Table 1. Chemical Composition of Materials

Material	Al	Mg	V	Si Max.	S	P	Mn	Cu	Pb	Zn	Cr	C	Fe Max.	Ni	Ti	
Titanium (RC 130B)	4.0	—	—	—	—	—	4.0	—	—	—	—	0-10 max.	—	—	Bal.	N 0.02
Magnesium	—	99.0+ min.	—	—	—	—	—	—	—	—	—	—	—	—	—	—
Aluminum (1100-F)	Bal.	—	—	Si+Fe 1.0 max.	—	—	0.05 max.	0.02	—	0.10 max.	—	—	Si+Fe 1.00 max.	—	—	—
Aluminum (2011-T8)	Bal.	—	—	—	—	—	—	5.5	0.5	—	—	—	—	—	—	Bi 0.5
Aluminum (7075-T6)	Bal.	2.1-2.9	—	0.50	—	—	0.30 max.	1.2-2.0	—	5.1-6.1	0.18-0.41	—	0.70	—	0.20 max.	—
Copper	—	—	—	—	—	—	—	99.9+ min.	—	—	—	—	—	—	—	—
Brass (70-30)	—	—	—	—	—	—	—	69.71	0.07	30.21	—	—	0.01	—	—	—
Lapelloy	—	—	0.29	0.48	0.011	0.016	1.15	—	—	—	11.12	0.28	Bal.	0.12	—	Mo 2.84
Steel (SAE 4340)	—	—	—	0.2-0.35	0.04 max.	0.04 max.	0.6-0.8	—	—	—	0.7-0.9	0.38-0.43	Bal.	1.65-2.0	—	—

Table 2. Surface Preparation of Specimens

Series Number	Surface Finish	Preparation Process
1-16	Mechanically polished	(1) shaped (2) polished with 240, 1, and 2/0 polishing clothes successively
17	Oxidized	(1) mechanically polished as described above. (2) batch 1, submerged in 30% H_2O_2 for 2 hrs. at room temperature (3) batch 2, submerged in H_2O_2 for 16 hrs. at room temperature
18	Shot peened	(1) mechanically polished as described above (2) shot peened by P39 Steel shots at 75 psi air pressure for 3 minutes
19	Shot peened	Same as series 18, but P19 steel shot was used
20	Teflon coated	(1) mechanically polished as described above (2) Teflon sprayed on specimen, then baked at temperature of 400°F (3) specimens were coated by General Electric Co.
21	Tungsten carbide plated	(1) mechanically polished as described above (2) Tungsten carbide particles were carried by a supersonic wave and were embedded in the specimen (3) ground by a 100 grit size diamond wheel (4) thickness of coating was approximately 0.002" (5) Specimens were coated by Linde Air Product Co.
22	Aluminized	(1) mechanically polished as described above (2) specimen was aluminized in an argon atmosphere at 1350°F for four minutes and subsequently heated for 15 min. at 1900°F to allow diffusion (3) specimens were coated by Solar Aircraft Co.
23	Screen	(1) mechanically polished as described above (2) nickel-plated copper screen of 40 mesh size placed between the gripping pads and the specimen
24	Screen	Same as 23 only 80 mesh size screen used.

Table 3. Summary of Results

Series No.	Gripping Material	Hardness of Gripping Pads VHN	Hardness of Specimen VHN	Gripping Pressure Psi	Surface Finish of Specimen	Fretting Fatigue Strength, Psi	Remarks
1	——	——	354	——	Mech. Polished	89,000	Conventional Fatigue Test
2	Mg	39	"	15,000	"	85,000	Adjusted Fatigue Limit
3	Al (1100-F)	41	"	"	"	85,000	" "
4	Al (2011-T8)	126	"	"	"	80,000	
5	Al (7075-T6)	194	"	"	"	38,000	
6	Cu	96	"	"	"	72,000	
7	Brass (70-30)	117	"	"	"	30,000	
8	Ti (RC 130B)	354	"	"	"	36,000	
9	Lapelloy	207	"	40,000	"	24,000	
10	Steel SAE 4340	397	"	4,000	"	28,000	
11	" "	397	"	22,000	"	21,000	
12	" "	397	"	60,000	"	18,000	
13	" "	238	"	40,000	"	21,000	
14	" "	397	"	"	"	22,000	
15	" "	595	"	"	"	19,000	
16	" "	238	"	"	"	21,000	Argon Atmosphere
17	" "	238	——	15,000	Oxidized	50,000	
18	Al (7075-T6)	194	——	15,000	Shot Peened	55,000	
19	Steel SAE 4340	238	——	40,000	Shot Peened	48,000	
20	Steel SAE 4340	238	——	15,000	Teflon Coated	51,000	
21	Tungsten Carbide Plated Lapelloy	946	870	40,000	Tungsten Carbide Plated	21,000	
22	Aluminized Lapelloy	——	——	15,000	Aluminized	22,000	
23	Screen & Steel SAE 4340	——	354	40,000	Mech. Polished	44,000	Nickel Plated Copper Screen*
24	Screen & Steel SAE 4340	——	354	40,000	Mech. Polished	34,000	Nickel Plated Copper Screen**

* Nickel Plated copper screens of mesh size 40 were used as cushions or inserts between the gripping pads and the specimens.

** Same as above, except screens of mesh size 80 were used.

Table 4. X-Ray Diffraction Patterns of Fretting Debris

	Debris Data		Filing or Literature Data	
	d(A^o)	Estimated Relative Intensity	d(A^o)	Estimated Relative Intensity
			Magnesium*	
Series 2 Magnesium Gripping Pad	2.80	40	2.77	30
	2.63	30	2.60	25
	2.47	100	2.45	100
	1.91	15	1.90	20
	1.61	20	1.60	20
	1.48	30	1.47	20
	1.37	20	1.38	18
	1.35	20	1.34	13
	2.13**	100		
	1.50**	50		
			Magnesium Oxide*	
			2.11	100
			1.49	52
			Pure Aluminum*	
Series 3 Al 1100-F Gripping Pad	2.35	100	2.33	100
	2.04	50	2.02	40
	1.44	25	1.43	30
	1.23	25	1.22	30
			Copper*	
Series 6 Copper Gripping Pad	2.11	100	2.08	100
	1.83	50	1.81	53
	1.29	30	1.26	33
	2.56**	100		
	1.53**	25		
			Cuprous Oxide*	
			2.47	100
			1.51	27
			70-30 Brass ***	
Series 7 70-30 Brass Gripping Pad	2.84	25	2.83	30
	2.49	50	2.46	20
	2.12	100	2.12	100
	1.84	10	1.84	40
	1.64	10		

* literature data
** relative intensities estimated separately
*** filing data

Table 5. Composition of Fretting Debris Determined by X-Ray Diffraction Test

Test Series	Gripping Pad Material	Debris Compositions
2	Mg	Mg
3	Al 1100-F	Al
6	Cu	Cu, CuO
7	70-30 Brass	Brass, $2ZnO \cdot TiO_2$ *
9	Lapelloy Steel	$TiFe_2$ *

* data not conclusive

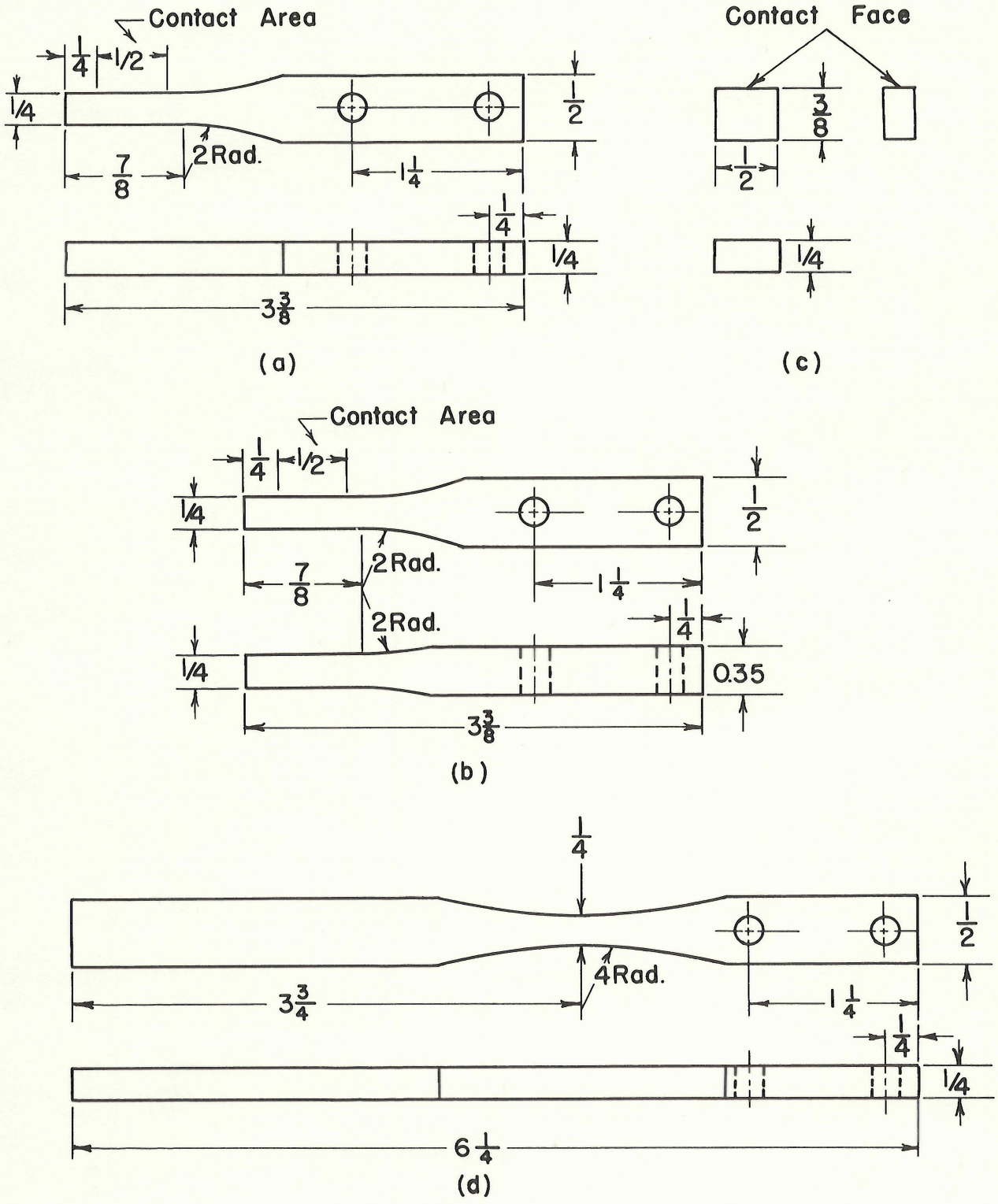

Note- All dimensions in inches.

Fig. 1 Fatigue Specimens and Gripping Pads

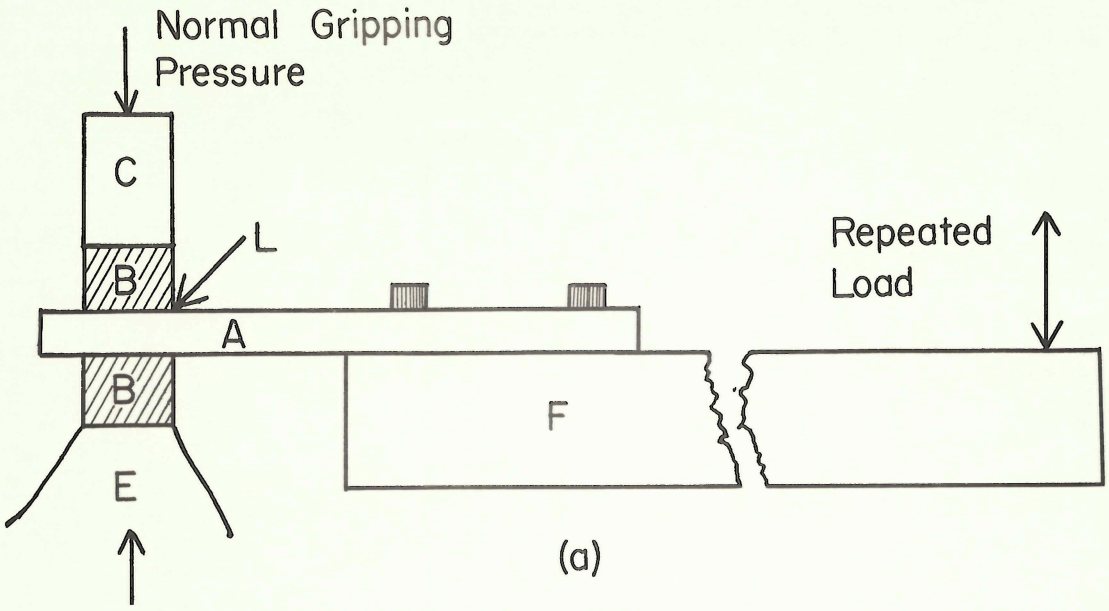

(a)

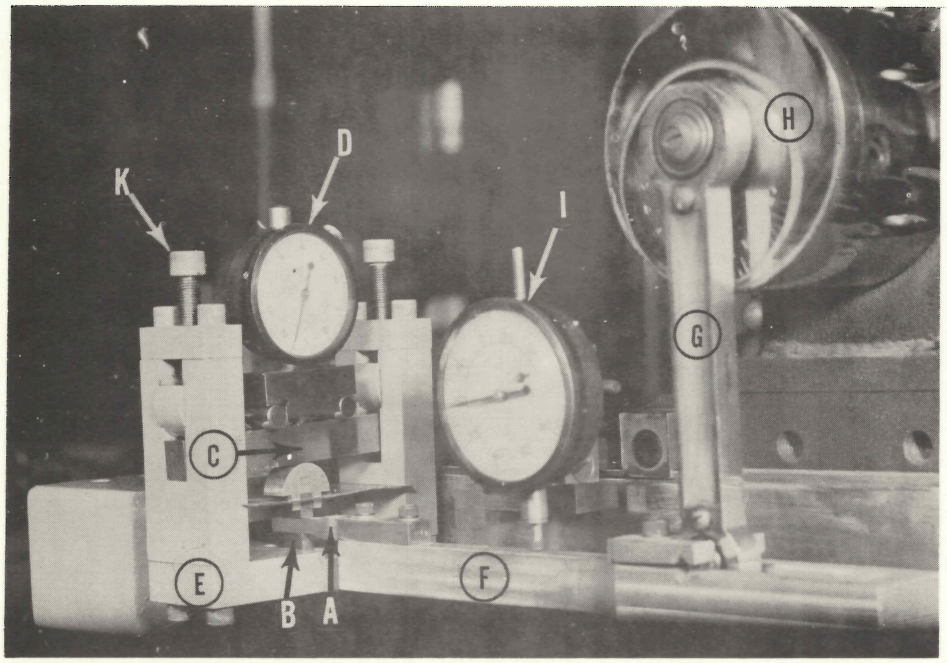

(b)

Fig. 2 (a) Schematic Diagram (b) Photograph of the Experimental Set-up. A--Specimen, B-Gripping Pads, C-Normal Pressure Loading Beam, D-Dial, E-Fixture Frame, F-Horizontal Loading Beam, G-Vertical Loading Beam, H-Eccentric Cam, I-Dial, K-Normal Pressure Adjusting Screw, L-Location of Maximum Slip.

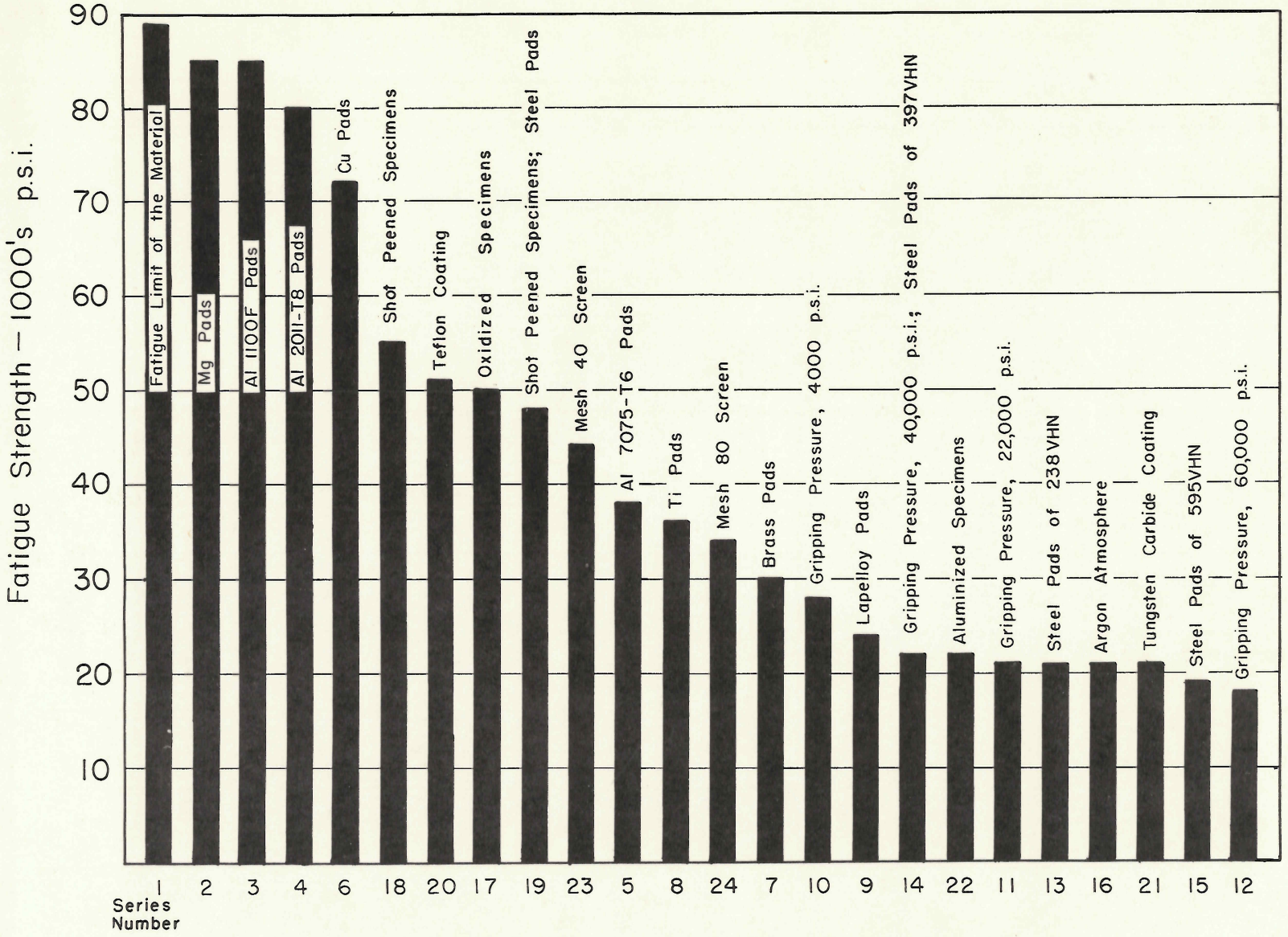

Fig. 3 Fretting Fatigue Strength of RC 130B Titanium Alloy under Various Experimental Conditions

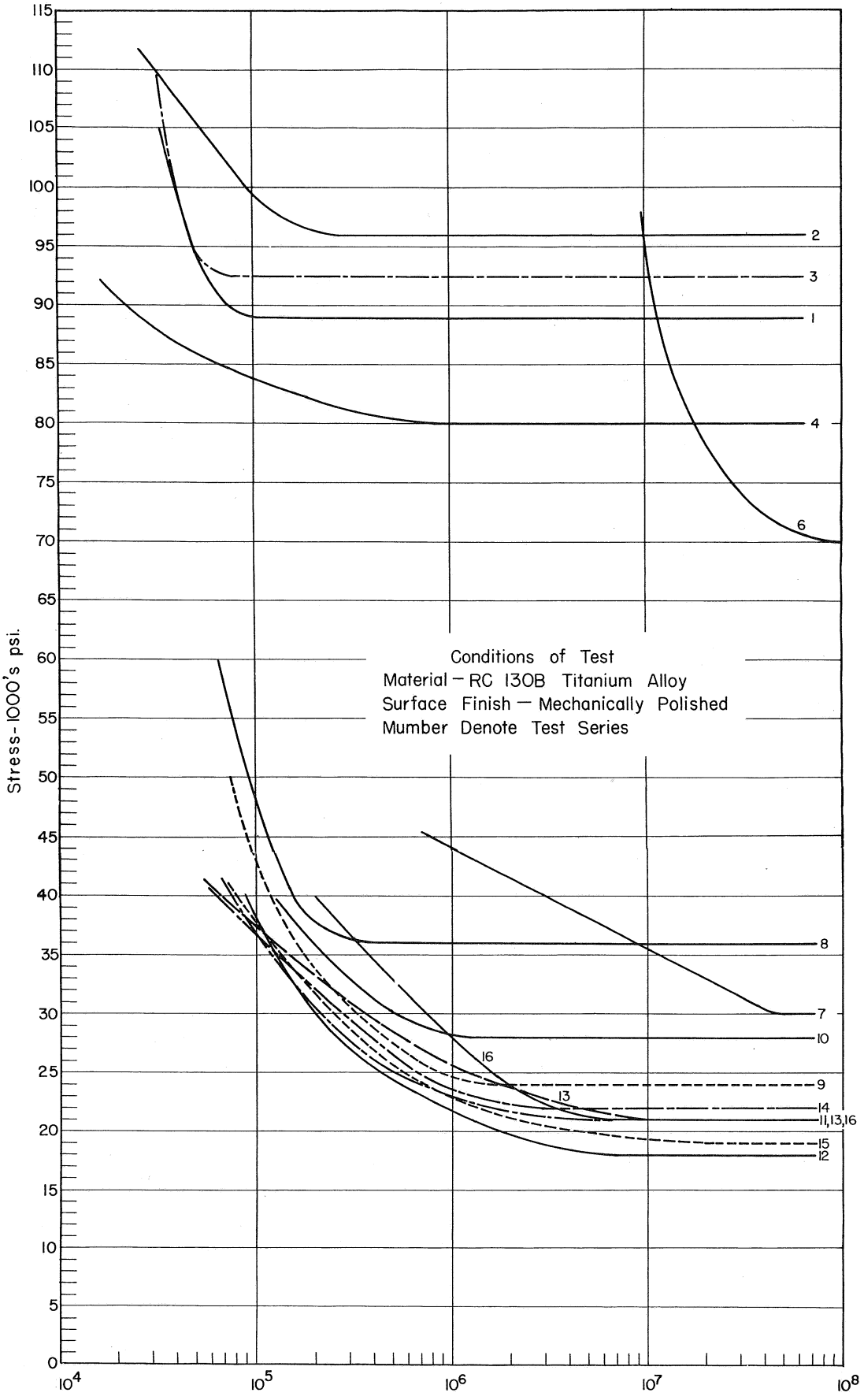

Fig.4 S-N Diagrams for Various Experimental Conditions

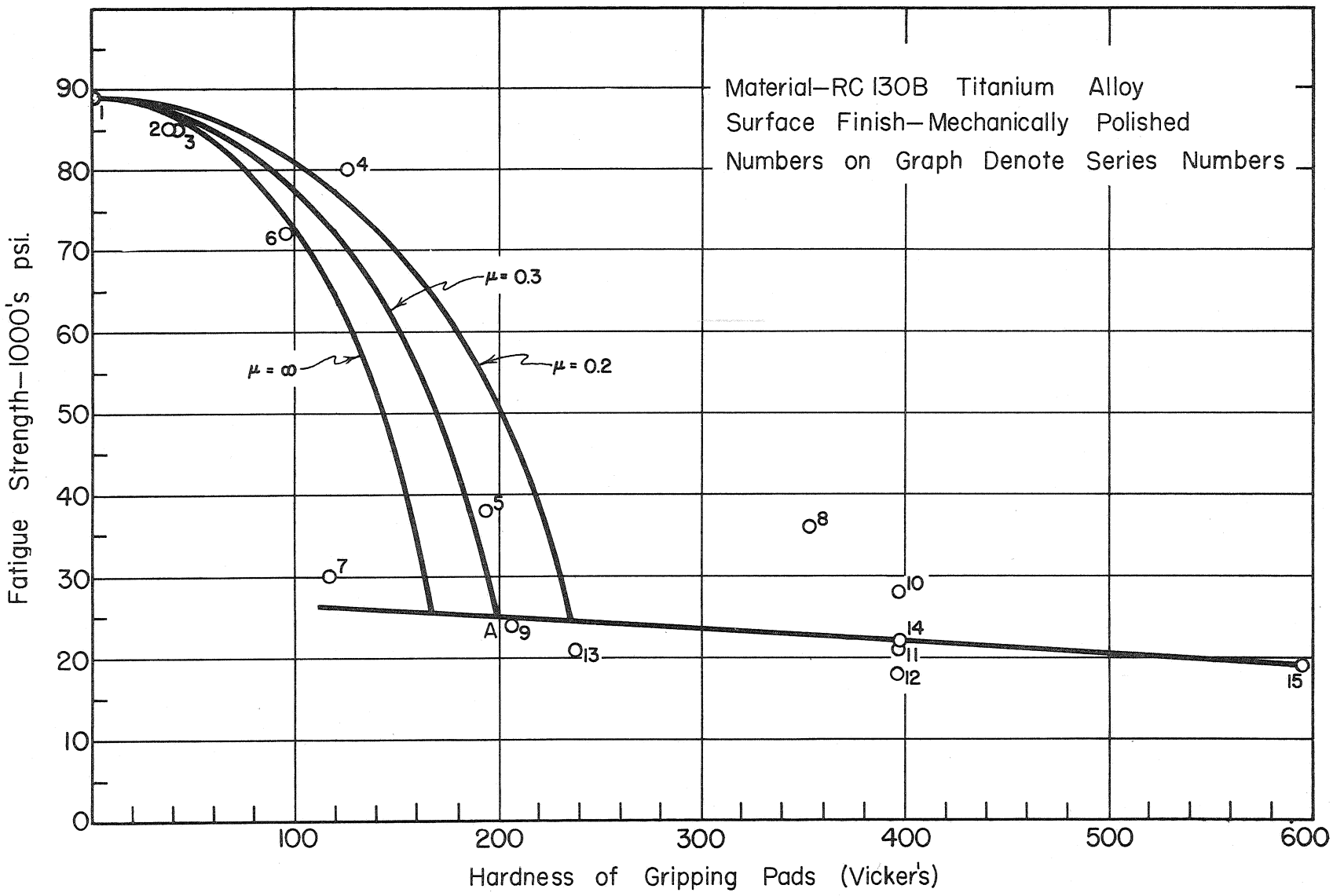

Fig. 5 Influence of Hardness of Gripping Pads on Fretting Fatigue Strength

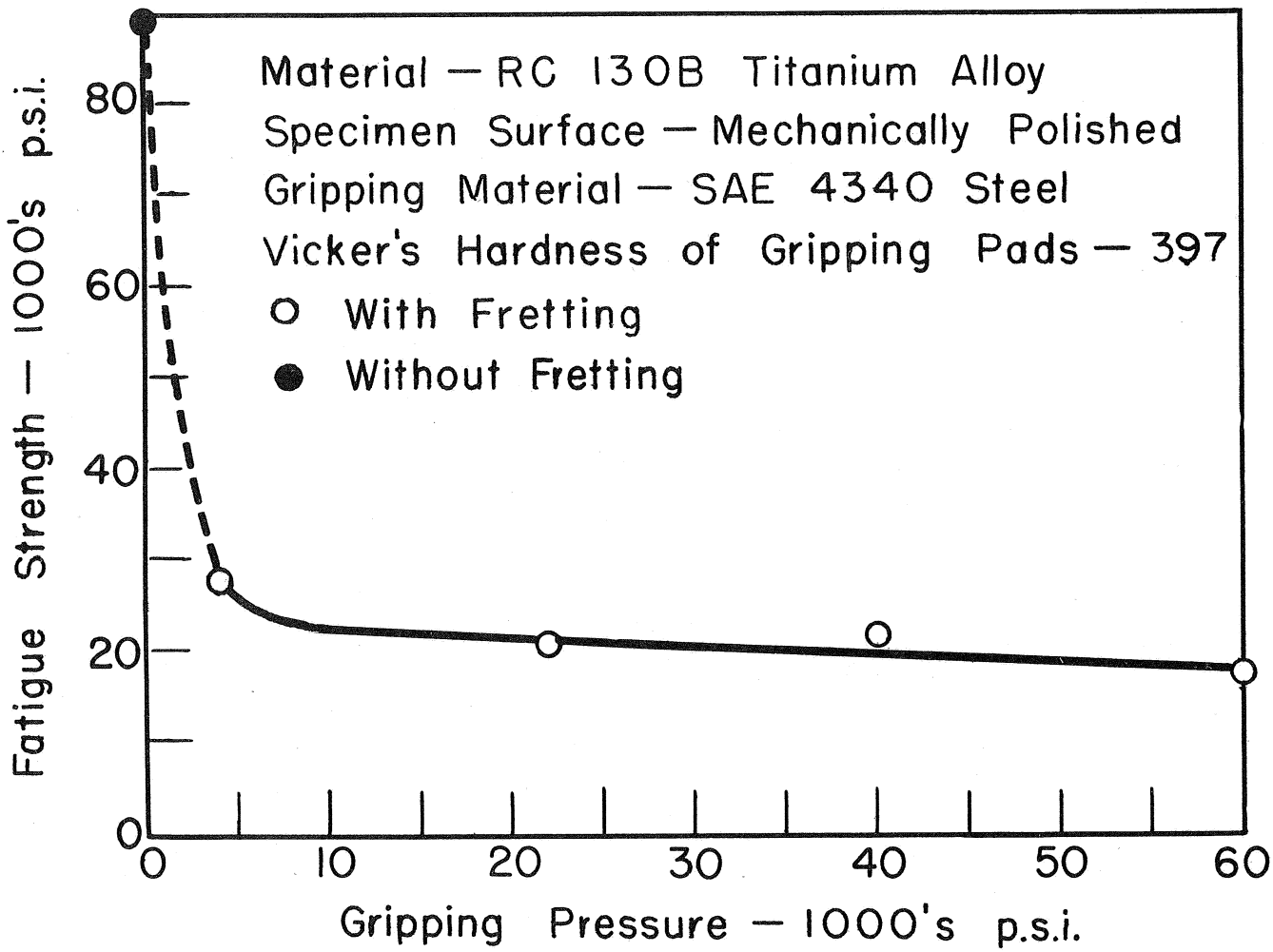

Fig. 6 Influence of Gripping Pressure on Fretting Fatigue Strength

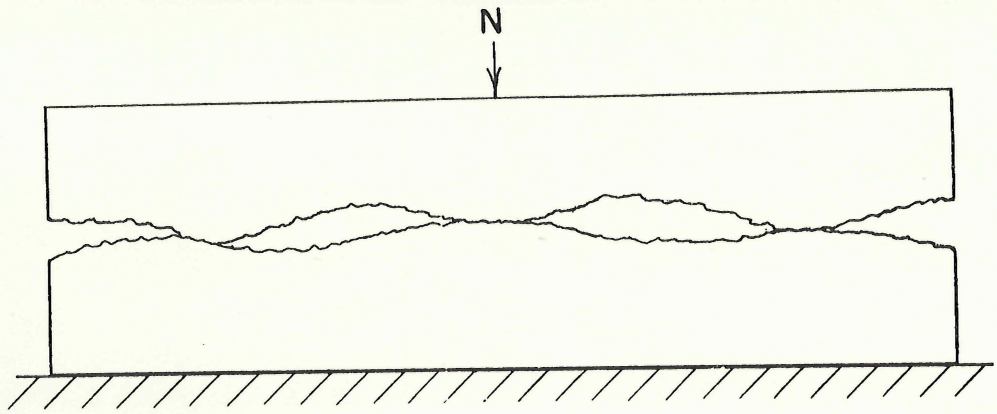

(a)

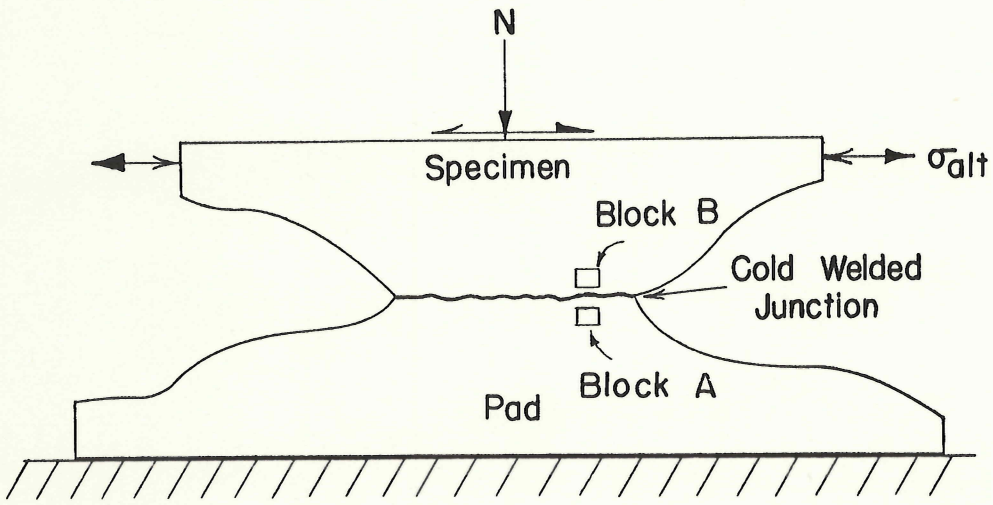

(b)

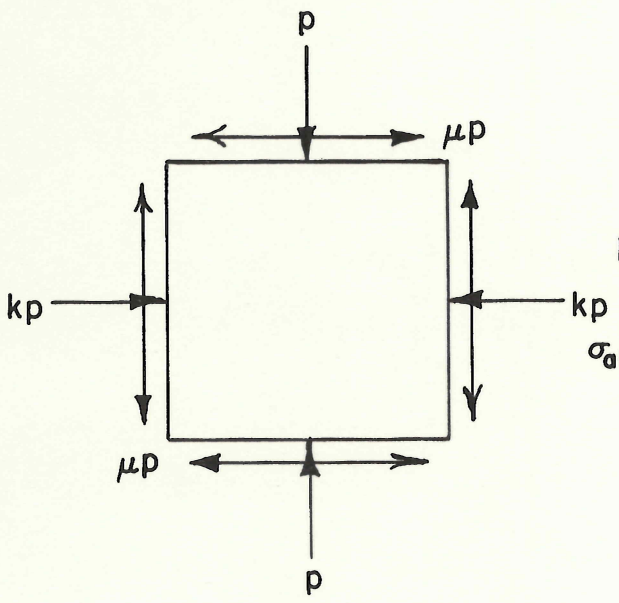

(c) Block A — Pad

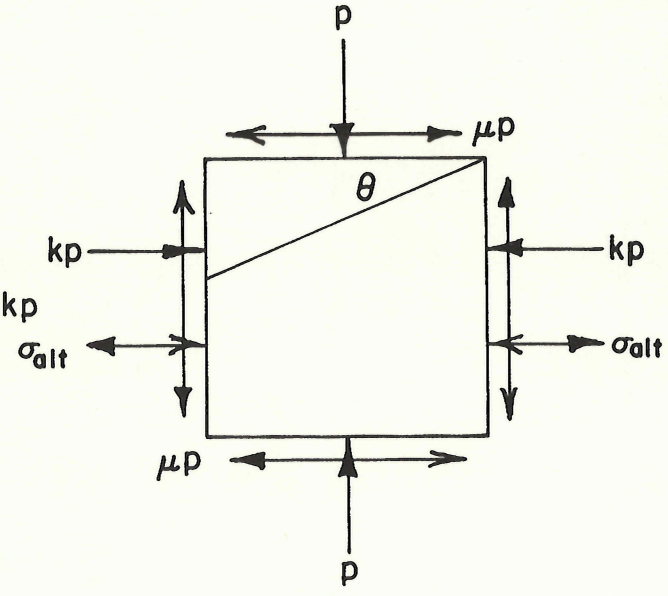

(d) Block B — Specimen

Fig. 7 Contacting Asperities and Associated Stresses

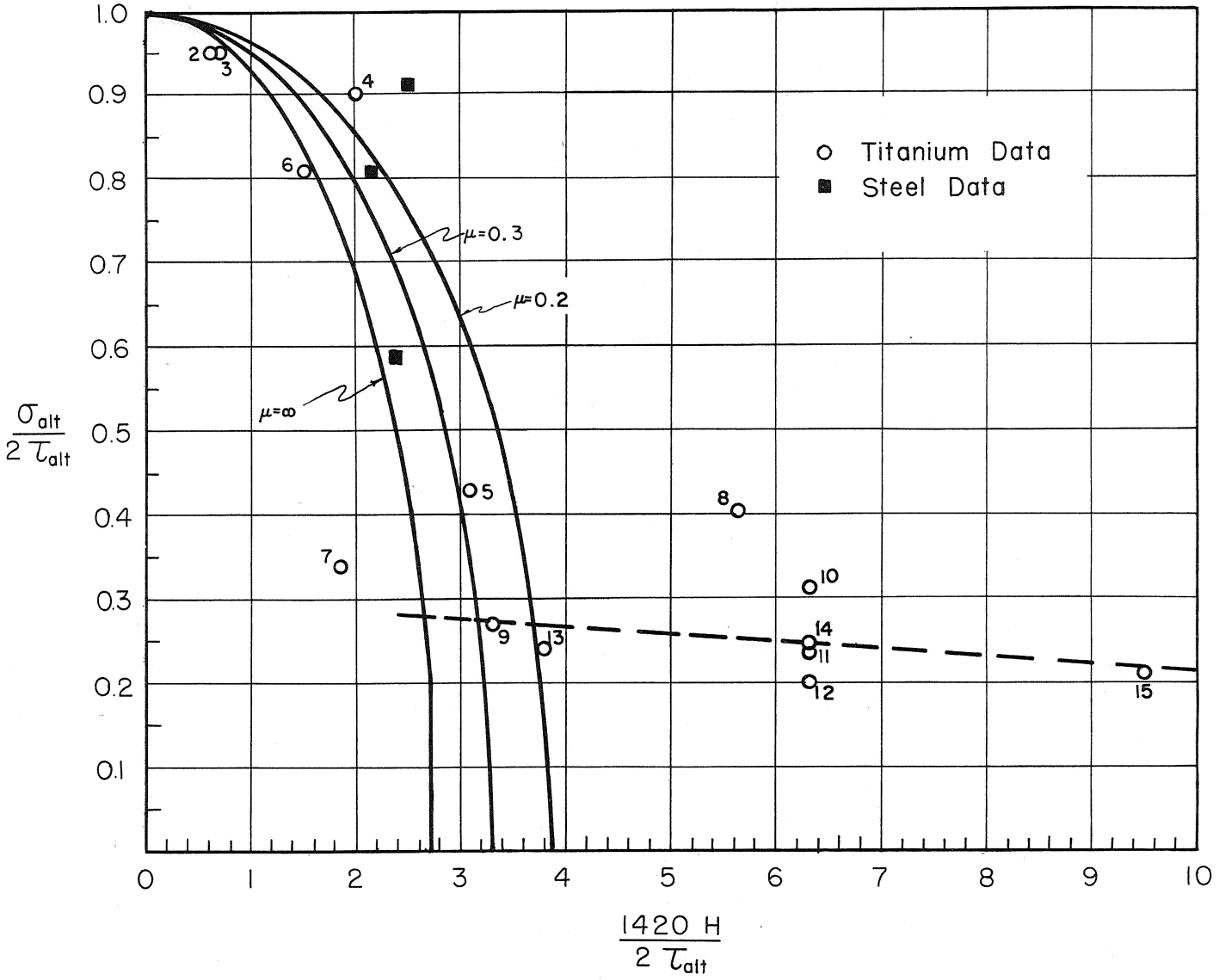

Fig. 8 Dimensionless Diagram Showing Fretting Fatigue Strength as Influenced by the Fatigue Limit of the Material, the Hardness of the Gripping Pads, and the Coefficient of Friction

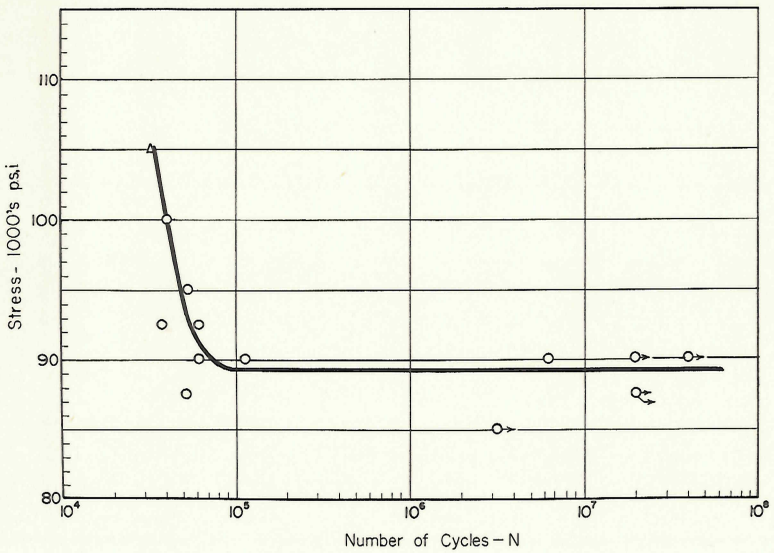

Fig. 9 S–N Curve for RC 130 B Titanium Alloy, Mechanically Polished Surface. Vickers Hardness of Specimen 354. Test Series 1

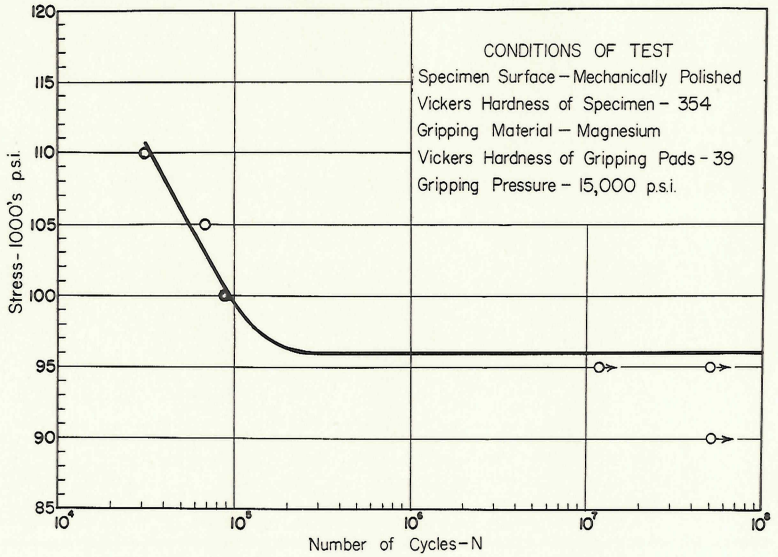

Fig. 10 Fretting Fatigue Data for RC-130 B Titanium Alloy, Test Series 2

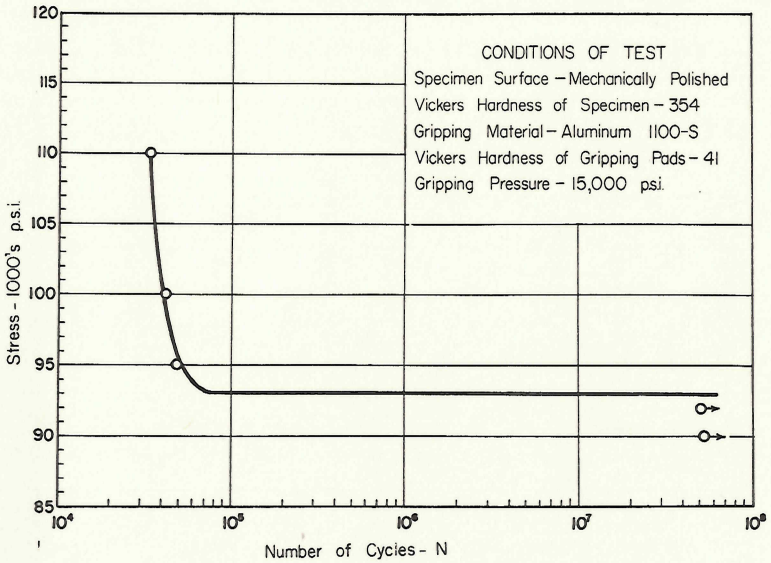

Fig. 11 Fretting Fatigue Data for RC-130 B Titanium Alloy, Test Series 3

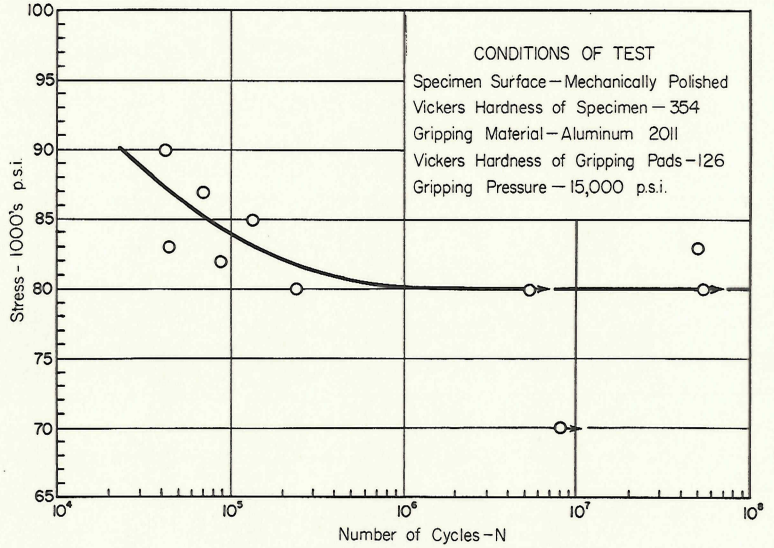

Fig. 12 Fretting Fatigue Data for RC-130 B Titanium Alloy, Test Series 4

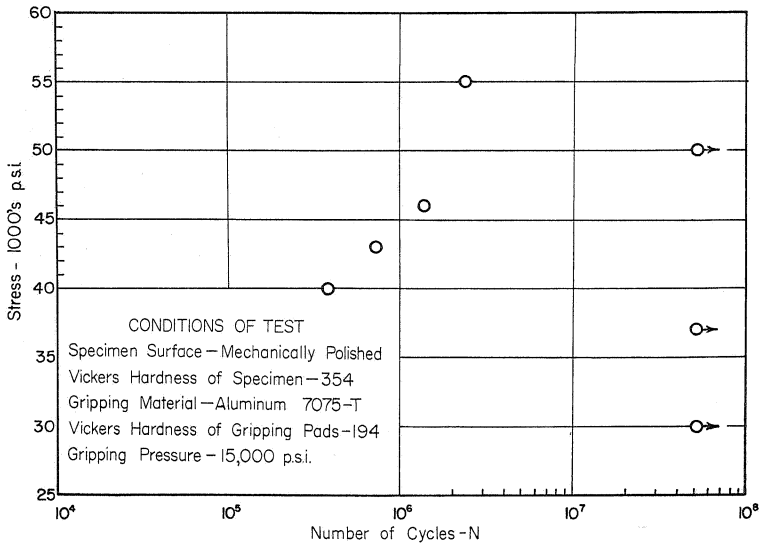

Fig.13 Fretting Fatigue Data for RC-130B Titanium Alloy, Test Series 5

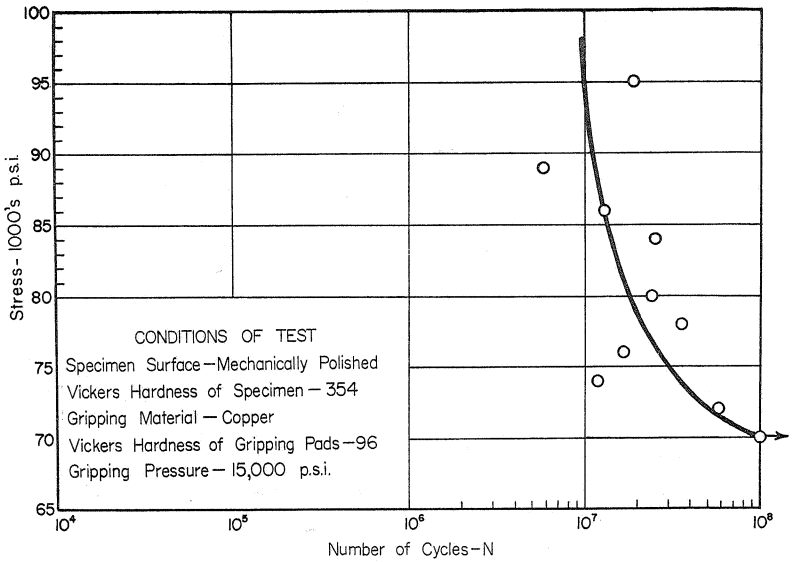

Fig.14 Fretting Fatigue Data for RC-130B Titanium Alloy, Test Series 6

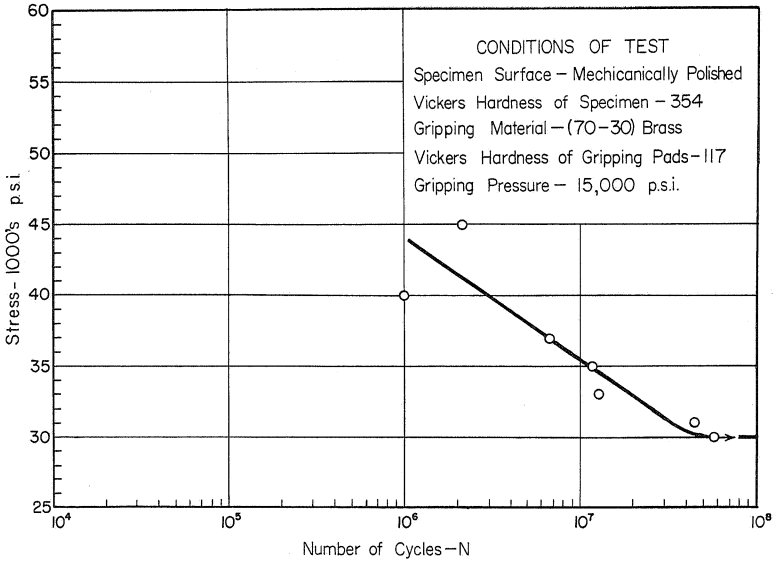

Fig.15 Fretting Fatigue Data for RC-130B Titanium Alloy, Test Series 7

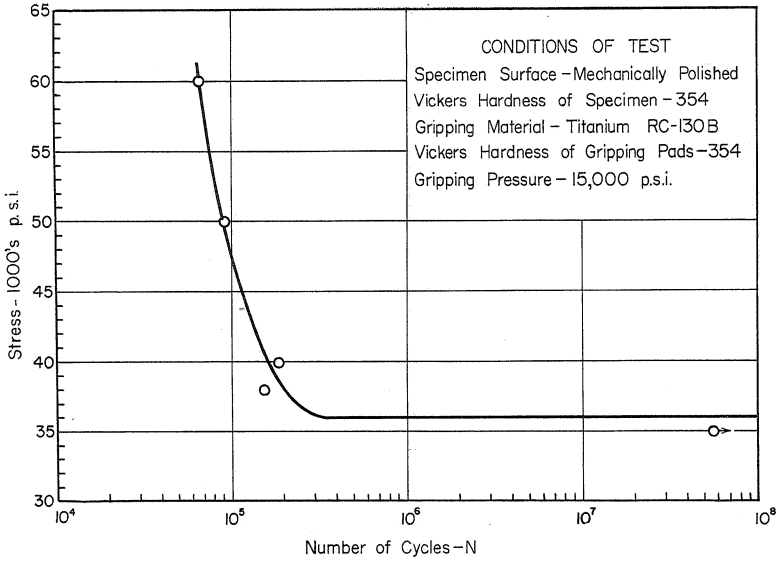

Fig.16 Fretting Fatigue Data for RC-130B Titanium Alloy, Test Series 8

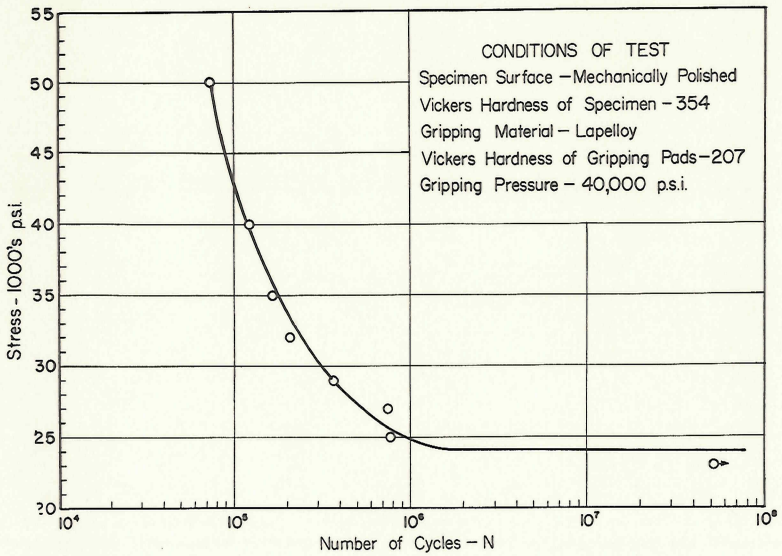

Fig.17 Fretting Fatigue Data for RC-130 B Titanium Alloy, Test Series 9

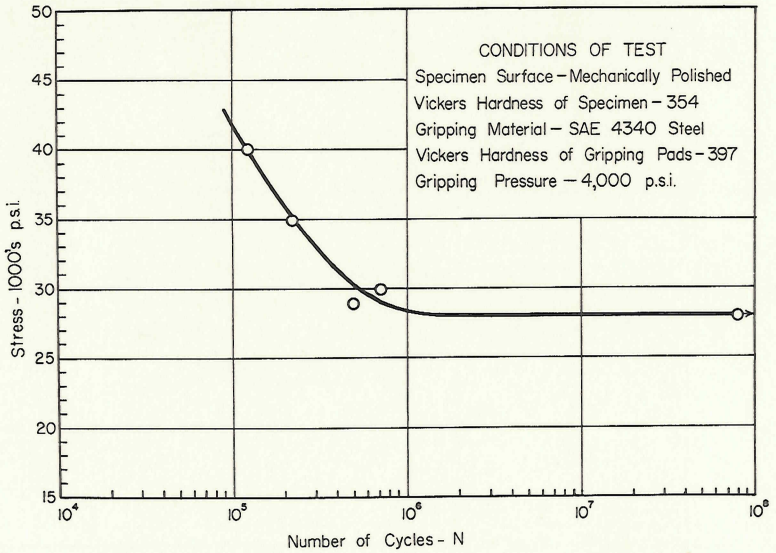

Fig.18 - Fretting Fatigue Data for RC-130B Titanium Alloy, Test Series 10

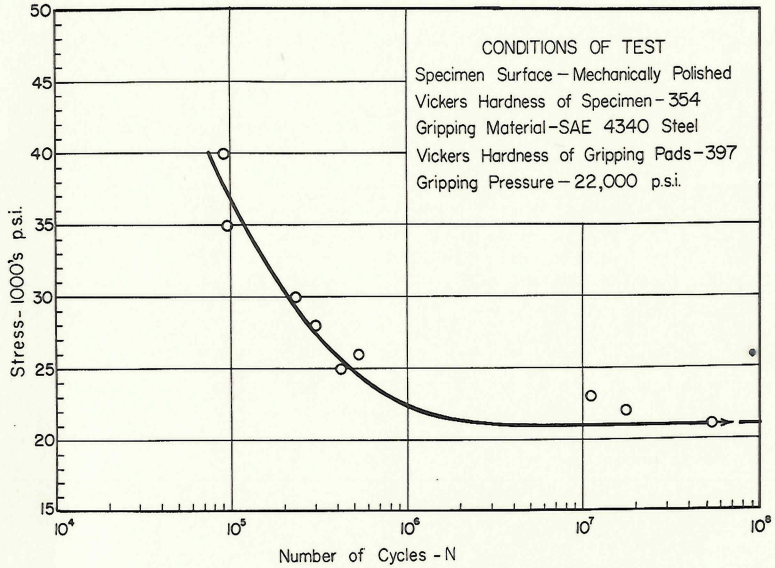

Fig.19 Fretting Fatigue Data for RC-130B Titanium Alloy, Test Series 11

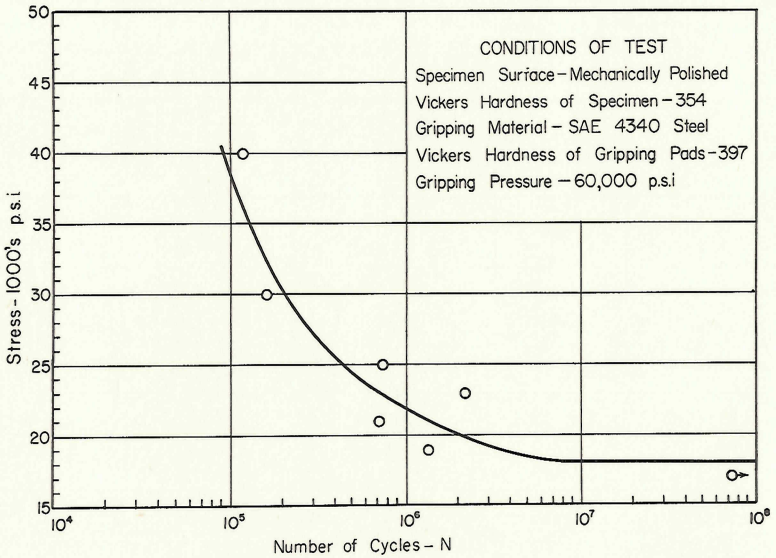

Fig.20 Fretting Fatigue Data for RC-130B Titanium Alloy, Test Series 12

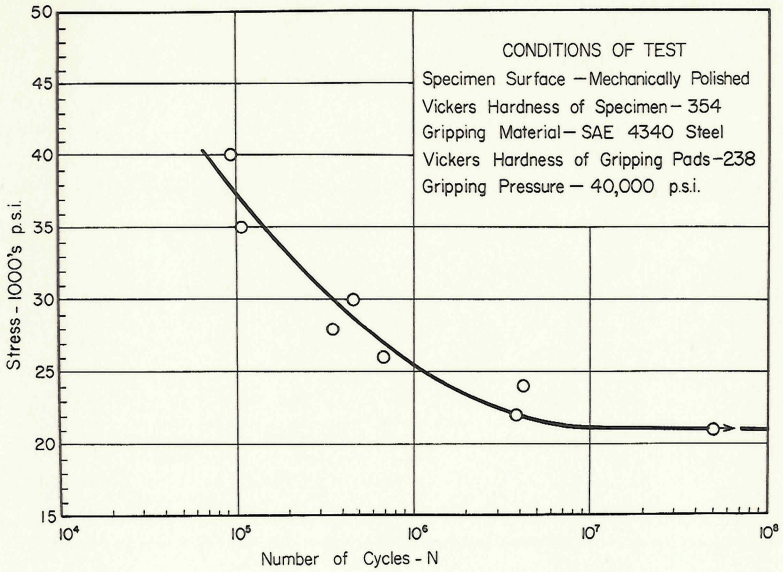

Fig.21 Fretting Fatigue Data for RC-130B Titanium Alloy, Test Series 13

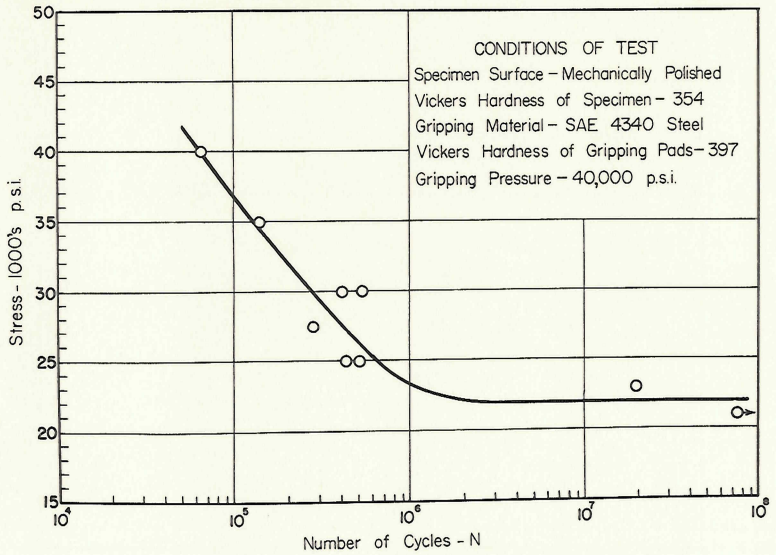

Fig.22 Fretting Fatigue Data for RC-130B Titanium Alloy, Test Series 14

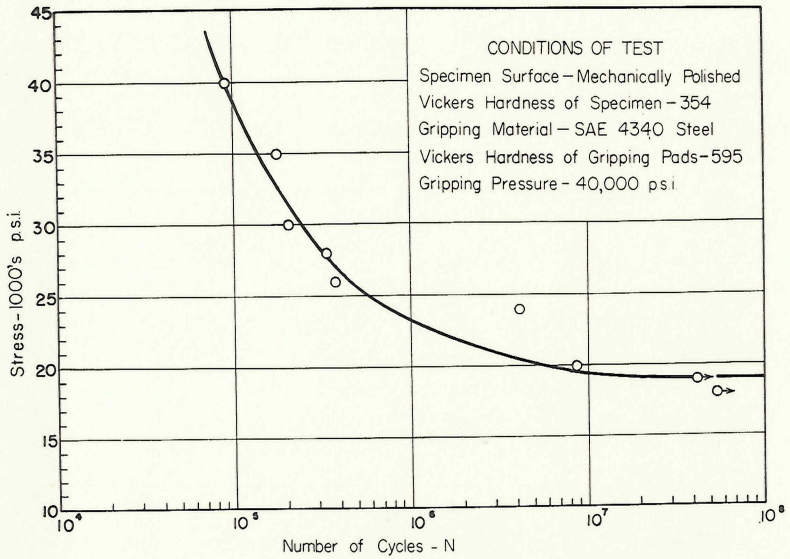

Fig.23 Fretting Fatigue Data for RC-130B Titanium Alloy, Test Series 15

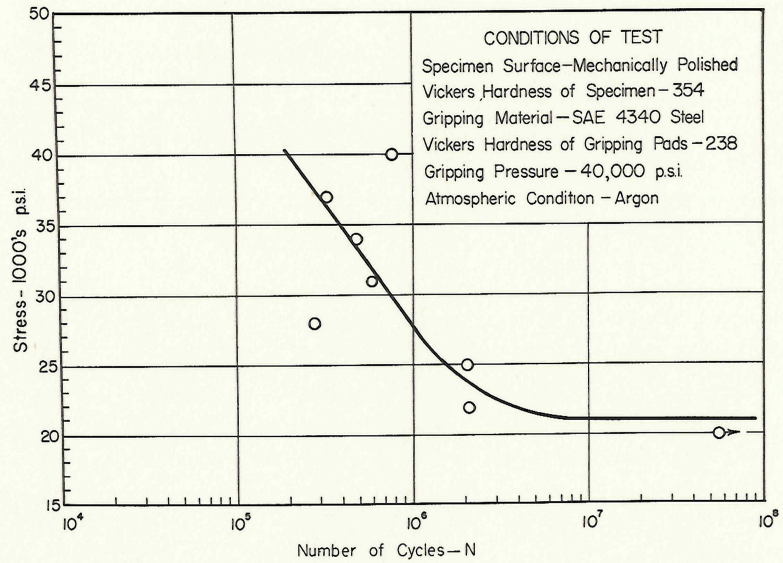

Fig.24 Fretting Fatigue Data for RC-130B Titanium Alloy, Test Series 16

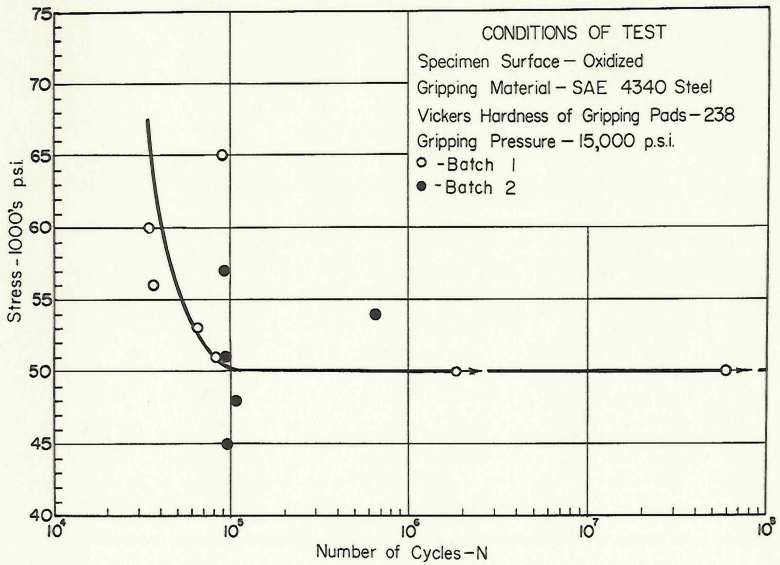

Fig.25 Fretting Fatigue Data for RC-130 B Titanium Alloy, Test Series 17

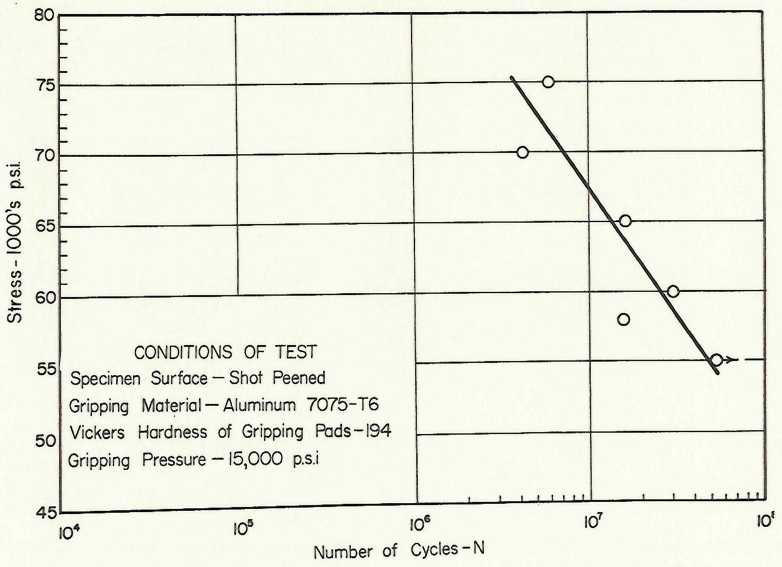

Fig.26 Fretting Fatigue Data for RC-130B Titanium Alloy, Test Series 18

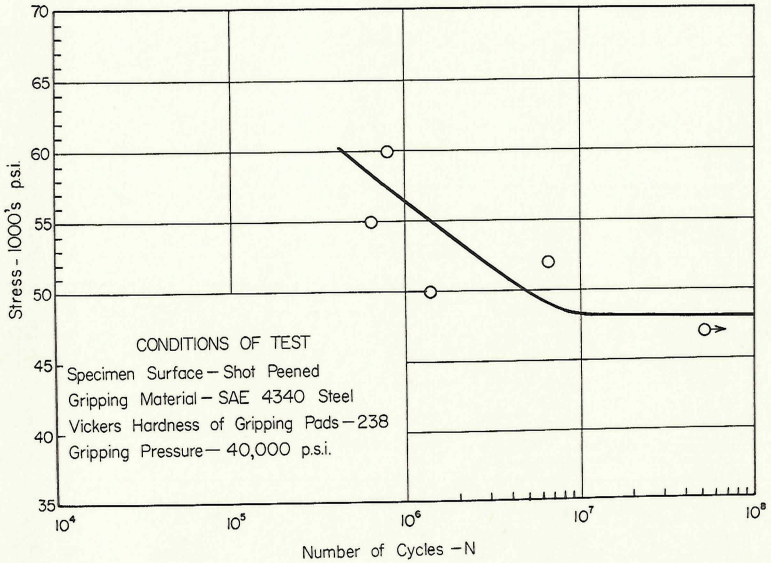

Fig.27 Fretting Fatigue Data for RC-130 B Titanium Alloy, Test Series 19

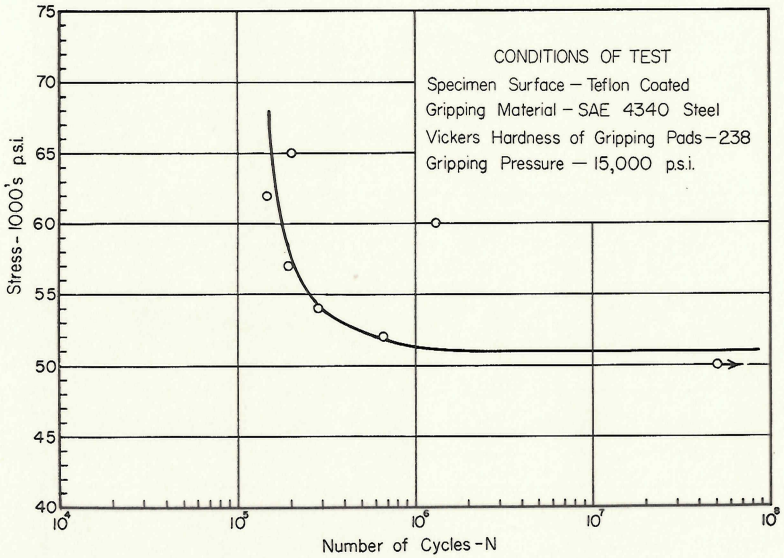

Fig.28 Fretting Fatigue Data for RC-130B Titanium Alloy, Test Series 20

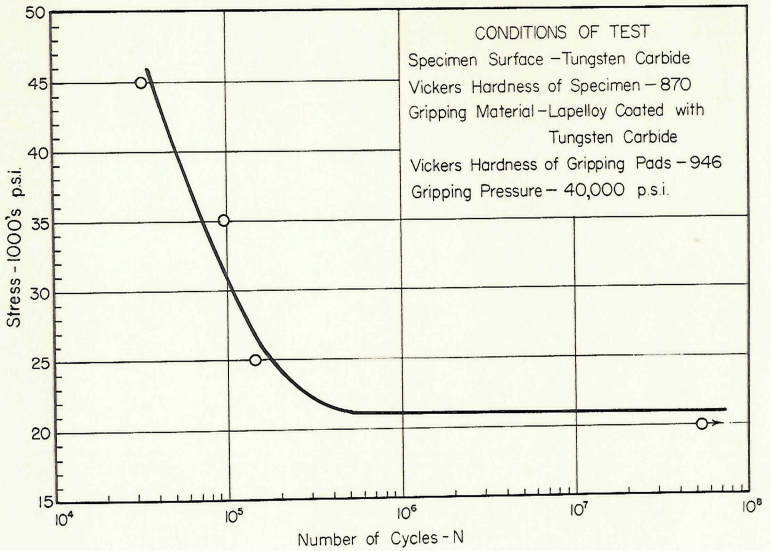

Fig.29 Fretting Fatigue Data for RC-130B Titanium Alloy, Test Series 21

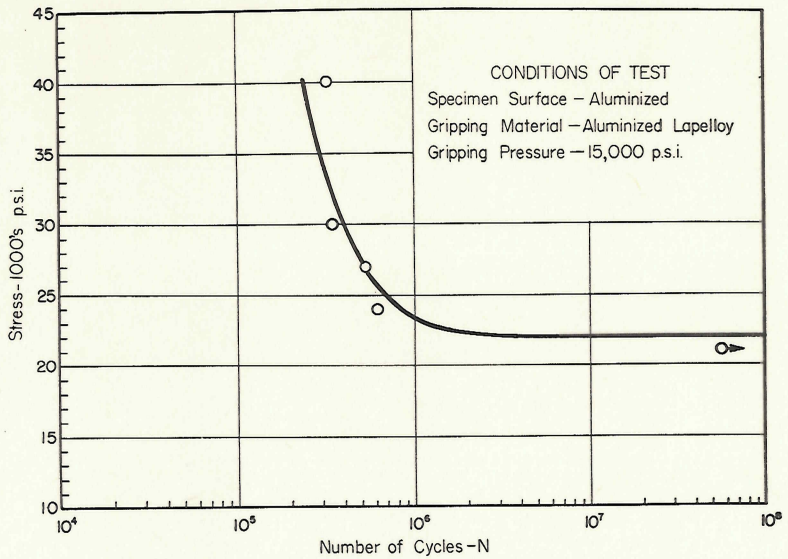

Fig.30 Fretting Fatigue Data for RC-130B Titanium Alloy, Test Series 22

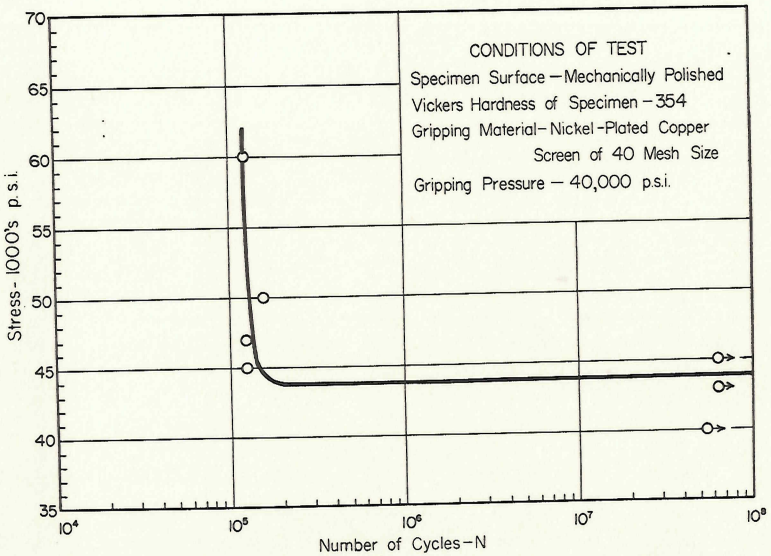

Fig.31 Fretting Fatigue Data for RC-130B Titanium Alloy, Test Series 23

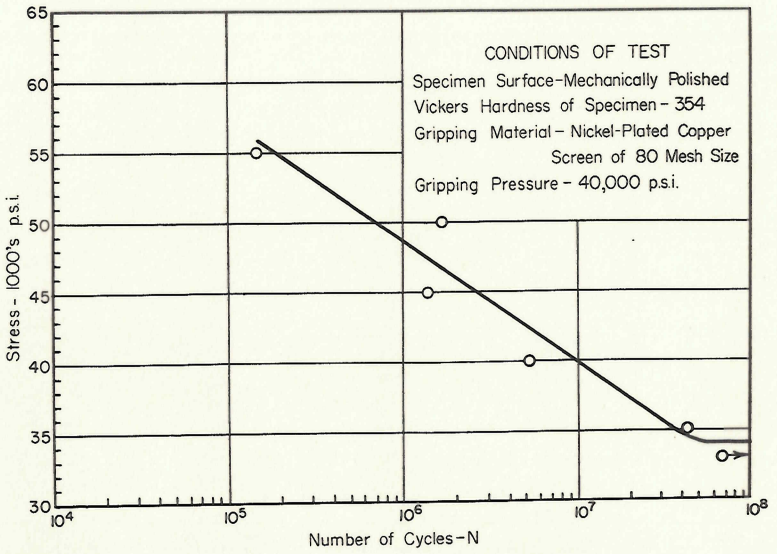

Fig.32 Fretting Fatigue Data for RC-130B Titanium Alloy, Test Series 24